Construction and Building Materials 194 (2019) 322–343

Contents lists available at ScienceDirect

Construction and Building Materials

journal homepage: www.elsevier.com/locate/conbuildmat

Experimental and numerical study on FRP-upgraded RC beams with large rectangular web openings in shear zones

Hussein M. Elsanadedy *[,1], Yousef A. Al-Salloum, Tarek H. Almusallam, Abdulhafiz O. Alshenawy, Husain Abbas

Chair of Research and Studies in Strengthening and Rehabilitation of Structures, Dept. of Civil Eng., College of Eng., King Saud University, P.O. Box 800, Riyadh 11421, Saudi Arabia

HIGHLIGHTS

- The effect of large rectangular openings in shear zone of FRP-upgraded RC beams is studied.
- Seven RC beams were prepared and tested under four-point bending until failure.
- There were one solid beam and six beams with two rectangular web openings in shear zones.
- Two opening sizes and two different strengthening schemes were investigated.
- Non-linear finite element analysis was conducted using LS-DYNA software.

ARTICLE INFO

Article history:
Received 26 March 2018
Received in revised form 17 September 2018
Accepted 31 October 2018
Available online 12 November 2018

Keywords:
RC beams
Openings
Shear strengthening
FRP
Steel plates
FE modeling

ABSTRACT

This paper studies experimentally and numerically the effect of large rectangular web openings in the shear zone on the response of unstrengthened and upgraded reinforced concrete (RC) beams. Studied parameters were opening size and strengthening scheme. Seven simply supported RC beams were prepared and tested under the action of two point loads. Beams comprised of one reference specimen without opening (i.e. solid beam) and six beams constructed with two large rectangular web openings, symmetrically located near supports. Out of the six beams with openings, two specimens were unstrengthened and four beams were strengthened with two fiber reinforced polymer (FRP) strengthening schemes. In one of the schemes, beams were strengthened using two layers (0°/90°) of carbon FRP (CFRP) sheets. However, the second scheme was a hybrid system comprising of glass FRP (GFRP) sheets anchored with bolted steel plates. The numerical models were prepared and the results of finite element (FE) analysis were validated with experiments. The validated numerical analysis was then used for some useful parametric studies in which the effect of different parameters was investigated.

1. Introduction

In reinforced concrete (RC) building frames, web openings are frequently provided in RC beams for passing ducts to accommodate vital utilities that may include air conditioning, electricity, telephone, water supply, and system network. These openings may be rectangular, circular, trapezoidal, triangular, diamond and sometimes irregular in shape. Nevertheless, the most common openings are rectangular and circular [1]. Web openings can be located in either high shear zones such as areas close to the column support in RC beams or high flexure zones such as areas near mid-span of beams. Many researchers have used the terms "small" and "large" openings for their classification without any clear distinction. Mansur [2] suggested the criteria to classify the size of openings. Author classified the web opening as small if $\ell_o \leq h_c$ where ℓ_o is the length of the opening and h_c is the larger of h_b and h_t; where h_b and h_t are the depths of bottom and top chords, respectively (see Fig. 1). For large opening, $\ell_o > h_c$.

Creating an opening in a beam introduces weakness, which causes reduction in the flexural stiffness and shear strength and increases the beam deflection at service load [2–4]. A planned opening in the RC beam can be taken care of at the design stage by providing extra rebars around it. Whereas, if it is decided to provide an opening in the beam at post-construction stage, the opening zone needs to be strengthened for avoiding premature beam failure. Fiber reinforced polymer (FRP) has been found to be effective for strengthening RC members in structures because of its excellent mechanical properties [5–16]. Several studies are available in

* Corresponding author.
E-mail address: elsanadedy@yahoo.com (H.M. Elsanadedy).
[1] On leave from Helwan University, Cairo, Egypt.

https://doi.org/10.1016/j.conbuildmat.2018.10.238
0950-0618/

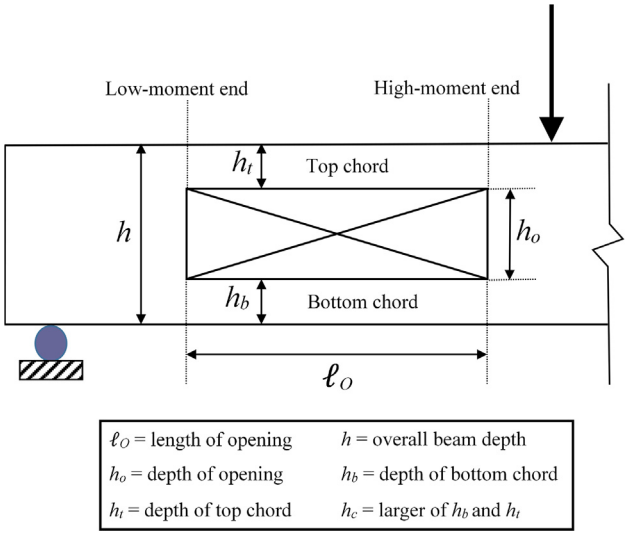

Fig. 1. Rectangular web opening in shear span of a simply supported RC beam.

literature for studying the behavior of FRP-upgraded solid RC beams (without openings) [16–18]. However, limited research is available on FRP-upgraded RC beams with web openings.

Abdalla et al. [19] studied the effect of the amount and configuration of the FRP in strengthening RC beams having web openings in the shear zone. Ten simply supported beams were tested and an analytical method was developed for the estimation of the beam strength. The test results revealed the effectiveness of the strengthening technique in controlling deflection and cracking, and improving the load carrying capacity.

Pimanmas [20] investigated experimentally and numerically the strengthening of the opening zones in RC beams using FRP rods. Thirteen beams having circular and square openings were tested. Two strengthening schemes using FRP rods were adopted. In one of the schemes, FRP rods were placed diagonally along the beam depth and in the other scheme the FRP rods were placed around the opening. It was reported that placing of FRP rods enclosing the openings was not very effective. However, the placement of FRP rods along the beam depth led to a substantial increase in the ultimate strength and ductility. A nonlinear finite element (FE) analysis was also conducted for numerical validation.

El Maaddawy and Sherif [21] tested thirteen deep beams with square web openings to study the effect of opening size, opening location, and FRP strengthening on the behavior of deep beams. Authors developed analytical models to assess the strength of CFRP-strengthened deep beams with openings. The study revealed the effectiveness of the CFRP strengthening system in restoring the shear strength of the deep beams.

Hawileh et al. [22] developed FE models using 8-node solid and 2-node link elements, respectively, to represent concrete volume and steel rebars in order to study the behavior of strengthened RC deep beams having openings. The strengthening in shear was done using CFRP composites. The CFRP sheets were modeled using multi-layer shell elements. The interfacial bond between concrete and CFRP laminates was modeled using special interface elements. The FE results were compared with experimental data available in the literature. The results of analysis showed the effectiveness of the numerical models in simulating the structural response of the unstrengthened as well as the CFRP-strengthened deep beams with openings.

Nie et al. [23] recently tested eight full-scale RC beams under center-point loading up to failure. Two specimens (one with rectangular section and one with T-section) were solid beams without openings and the remaining six beams were built with T-section and had single rectangular web opening in shear zone. Out of the six T-beams with openings, two beams were unstrengthened and six beams were strengthened with externally bonded CFRP sheets. Test results showed that a sizable web opening can reduce the flexural strength of the T-beam and the CFRP strengthening system is needed for avoiding shear failure and for confining the web chord created by the opening to ensure a ductile response.

The aim of this research is to study experimentally and numerically the effect of large rectangular web openings in the shear zone on behavior of unstrengthened and strengthened RC beams. Studied parameters included opening size and strengthening scheme. A total of seven simply supported RC beams were prepared and tested under the application of two point loads. Two different opening sizes as well as two different strengthening schemes were investigated. The numerical analysis was performed using the FE software LS-DYNA [24]. The numerical and experimental results were compared. The validated numerical analysis was then used for some useful parametric studies in which the influence of various parameters including the opening size and the strengthening schemes were investigated.

2. Experimental program

2.1. Test matrix

The experimental program comprised of seven RC beams with section dimensions of 200 × 450 mm tested under four-point bending. The test matrix, providing the details of experiments, is given in Table 1. One beam without opening was used as a control for making comparisons with other beams. The remaining six beams were divided into two groups of three RC beams each. In the first group, beams were constructed with two rectangular openings of 225 mm depth and 450 mm length. However, in the second group, the opening length was increased to 675 mm. The first beam of each group was kept unstrengthened. The second beam was upgraded using two layers (0°/90°) of externally bonded CFRP sheets. However, the third beam of each group was strengthened using a hybrid scheme comprising of externally bonded GFRP sheets anchored with bolted steel plates. The effectiveness of the strengthening schemes was evaluated by comparing the response of the tested beams in terms of their modes of failure and load-deflection characteristics.

2.2. Test specimen details and preparation

The RC beams of rectangular cross-section (200 × 450 mm) and 3 m long were casted using the same amount of longitudinal rebars and shear stirrups. By keeping an overhang of 100 mm on each end, the effective span of the beam was 2800 mm.

Table 1
Test Matrix.

Beam ID	Opening size (mm)		Strengthening scheme	No. of specimens	Notes
	Depth, h_o	Length, ℓ_o			
BC-N	No opening		Unstrengthened	1	Control specimen
BC-O1	225	450	Unstrengthened	1	Control specimen
BS1-O1	225	450	2 layers (0°/90°) of carbon/epoxy system (Scheme-1)	1	
BS2-O1	225	450	2 layers (0°/90°) of E-glass/epoxy system + 5 mm thick steel plates (Scheme-2)	1	
BC-O2	225	675	Unstrengthened	1	Control specimen
BS1-O2	225	675	2 layers (0°/90°) of carbon/epoxy system (Scheme-1)	1	
BS2-O2	225	675	2 layers (0°/90°) of E-glass/epoxy system + 5 mm thick steel plates (Scheme-2)	1	
Total No. of specimens				7	

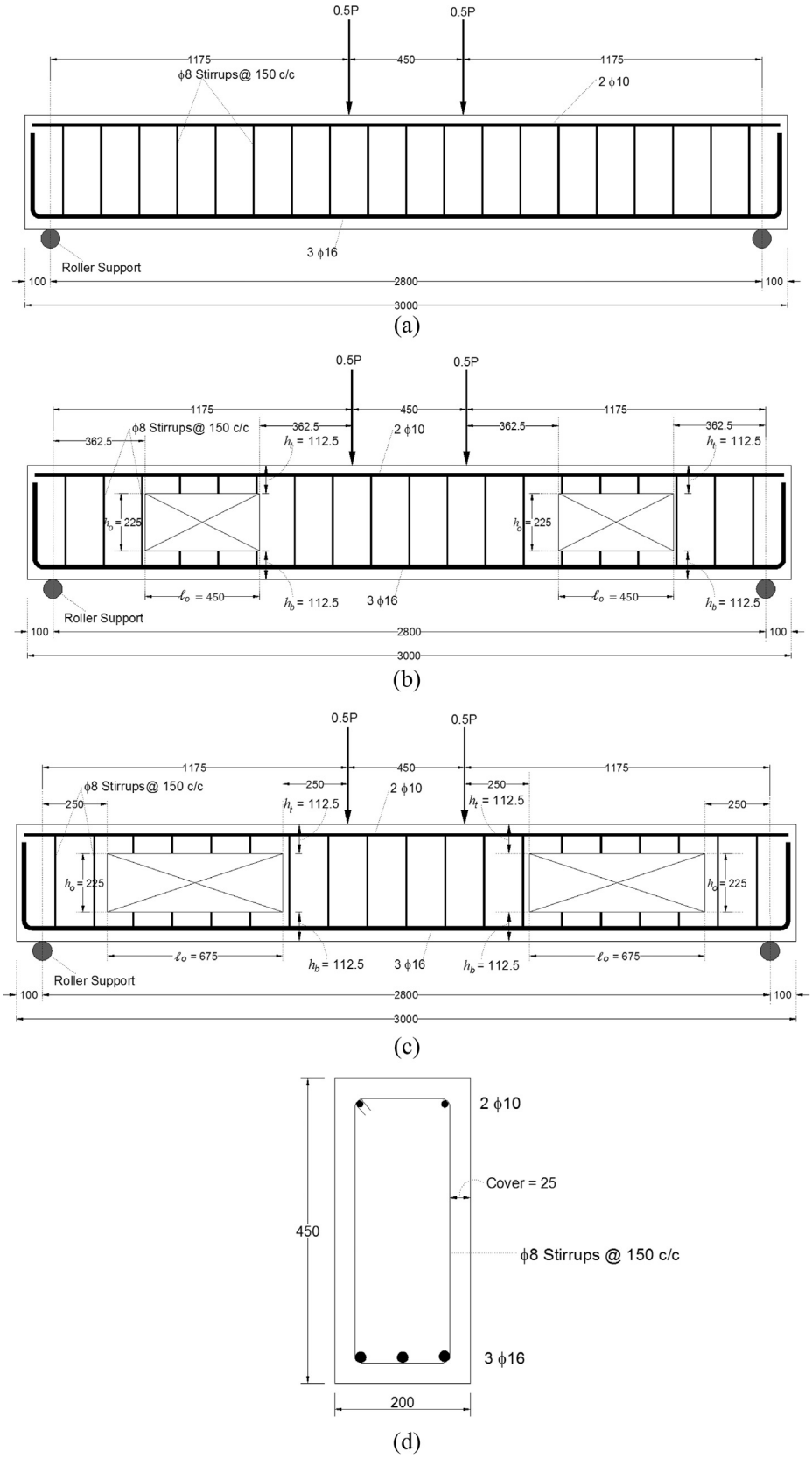

Fig. 2. Details of unstrengthened beams (Note: All dimensions are in mm): (a) Elevation of control beam BC-N; (b) Elevation of beam BC-O1; (c) Elevation of beam BC-O2; (d) Beam section.

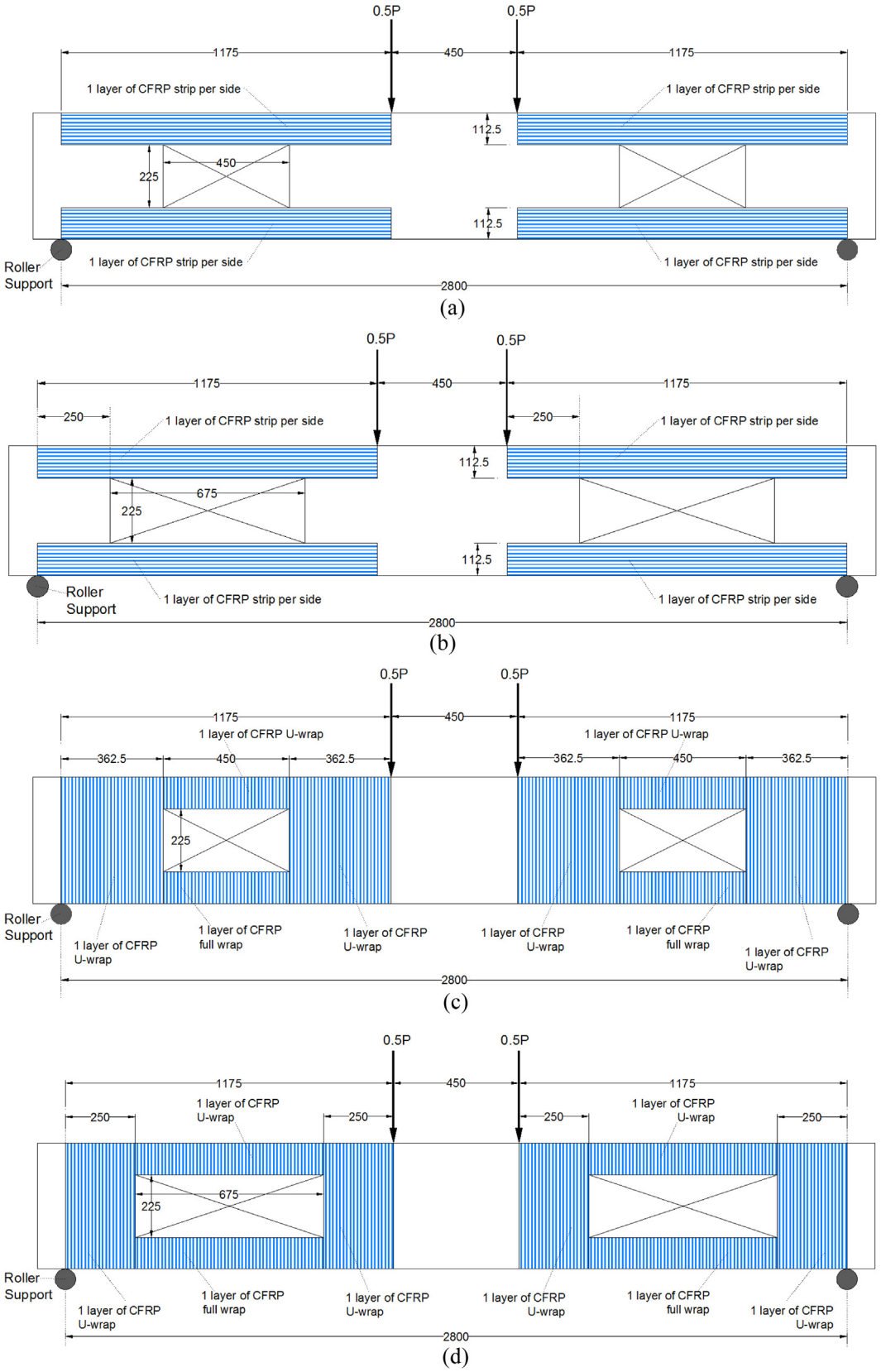

Fig. 3. Details of beams strengthened with scheme-1 (Note: All dimensions are in mm): (a) 1st CFRP layer of specimen BS1-O1; (b) 1st CFRP layer of specimen BS1-O2; (c) 2nd CFRP layer of specimen BS1-O1; (d) 2nd CFRP layer of specimen BS1-O2.

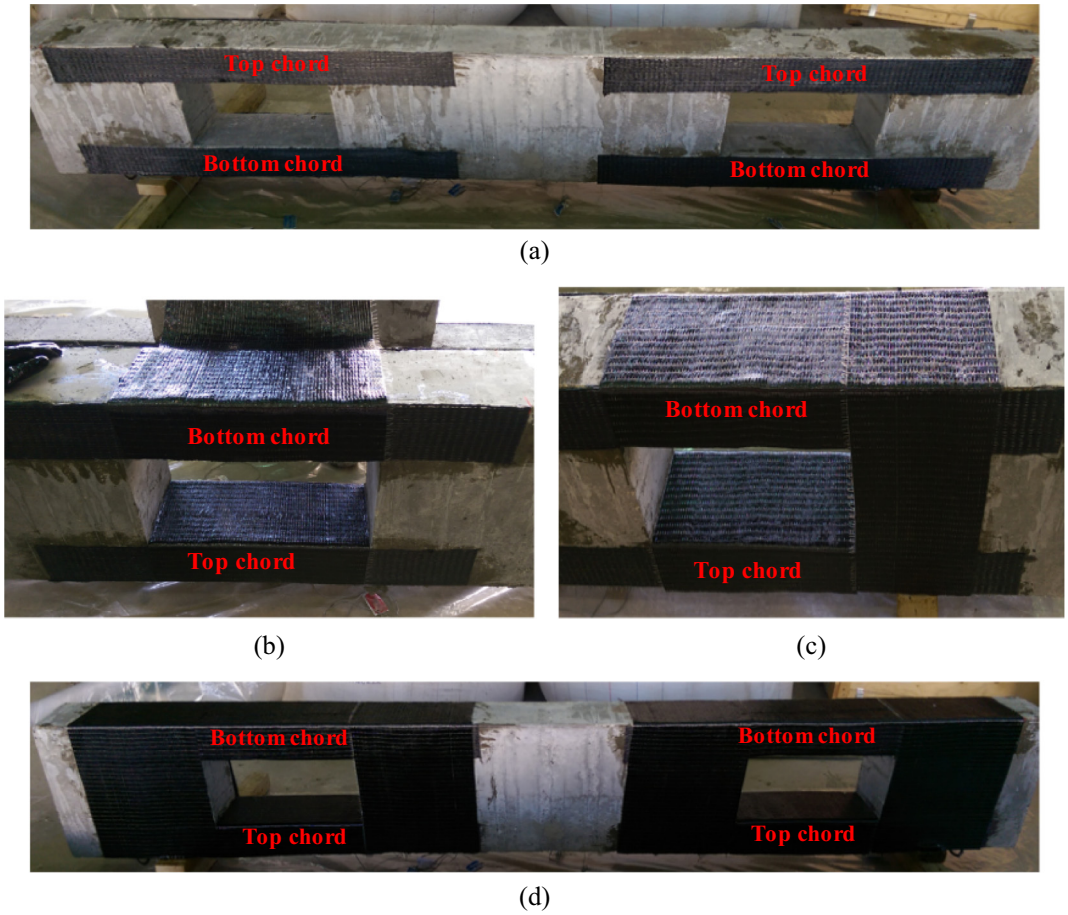

Fig. 4. Steps involved in strengthening of beams using scheme-1: (a) 1st CFRP layer is completed on both chords; (b) 2nd layer of CFRP U-wrap is completed for top chord and bottom chord is being fully wrapped with 2nd CFRP layer; (c) 2nd layer of CFRP U-wrap is completed on one opening side; (d) Strengthened beam ready for testing.

The size of test beams was chosen based on the available test facilities. The flexure steel was designed to have an under-reinforced section for causing tension failure. Details of unstrengthened RC beams are given in Fig. 2. The arrangement of reinforcement for all the beams consists of 3 ϕ16 mm rebars as longitudinal tension steel and 2 ϕ10 mm bars as compression reinforcement. Stirrups of ϕ8 mm @ 150 mm c/c spacing were provided as transverse reinforcement throughout the span. For beams with web openings, two large rectangular openings were constructed and they were located symmetrically, as shown in Fig. 2. For beams of the first group (BC-O1, BS1-O1 and BS2-O1), the length and depth of the openings were 450 and 225 mm, respectively. However, for beams of the second group (BC-O2, BS1-O2 and BS2-O2), opening length was 675 mm. As seen in Fig. 2, U-stirrups were provided in the opening zone thus representing the opening created on site by cutting stirrups in existing beams.

The strengthening schemes were designed once the flexural tests for the unstrengthened specimens were done and the failure patterns established. As mentioned earlier, two types of FRP strengthening schemes were designed in this study. The first scheme (scheme-1) involved the use of CFRP laminates and the second scheme (scheme-2) involved the use of GFRP laminates anchored using steel plates. Details of beams strengthened with scheme-1 (BS1-O1 and BS1-O2) are given in Fig. 3. In addition, steps involved in the strengthening of beams using scheme-1 are depicted in Fig. 4. As shown in Figs. 3 and 4, the first scheme comprised of applying two layers of CFRP sheets in the designated patterns. CFRP strips of 112.5 mm width (equal to the depth of top and bottom chords) were first applied on the two sides of both the chords of the beams, with the primary fiber oriented in the horizontal direction. The length of these strips was 1175 mm, as shown in Fig. 3(a) and (b). On top of these strips, the second layer of CFRP strip was affixed with the pattern shown in Fig. 3(c) and (d). The second layer comprised of four pieces of CFRP sheets having their fibers oriented along the beam depth, which were applied separately to the top and bottom chords, and on both sides of the opening. The top chord and the two sides were wrapped using a U-shape wrap, whereas the bottom chord was fully wrapped. The reason for this being that practically it would not be possible to wrap the top chord fully due to the presence of slab.

The second scheme of strengthening comprised of GFRP sheets together with steel plates. The purpose of using steel plates was to make sure the GFRP sheet was properly anchored to the beam and provides strength to the top chord. In this scheme, the reason for selecting GFRP instead of CFRP was to avoid the issue of galvanic corrosion, which arises because of metals connected to CFRP, so that this strengthening system could be used safely in the field. Details of beams strengthened with scheme-2 (BS2-O1 and BS2-O2) are given in Fig. 5. Furthermore, steps involved in the strengthening of beams using scheme-2 are shown in Fig. 6. The patterns of the second scheme were essentially the same as scheme-1 with only one exception. The first layer of GFRP strips was not applied to the top chords on either side of the beams. It was only applied to the bottom chords, as seen in Fig. 5. The second layer of GFRP pattern was exactly the same as scheme-1 (Fig. 5). After the GFRP sheets were applied and the epoxy completely hardened, 5 mm thick ASTM A36 steel plates were attached to the top chords, as shown in Fig. 5. Holes were first driven at regular intervals in the concrete beam through the GFRP sheet and 10 mm threaded rods passed through the holes. The space around the rods and concrete was completely closed with an epoxy adhesive mortar (Sika-41). Holes were driven in the steel plates and the beam where the threaded rods were located. The steel plate was passed through the rods and attached to the concrete surface. Epoxy adhesive mortar (Sika-41) was applied on the surface of the steel plate to fill in the gaps between the plate and the concrete. Pressure was applied until some of the epoxy squeezed from in-between the plate and GFRP-strengthened concrete surface. Nuts were then tightened on the 10 mm threaded rods thereby anchoring the steel plates to the GFRP-strengthened concrete surface strongly.

2.3. Material properties

Ready-mix concrete was utilized for casting the RC beams. The compressive strength of concrete obtained according to the ASTM C39 [25] on the test date was 50 MPa. For steel rebars, tensile tests were conducted as per ASTM E8/E8M [26] and the average values of yield and tensile strengths of ϕ8, ϕ10 and ϕ16 mm rebars are given in Table 2. For steel plates, standard tension test coupons were

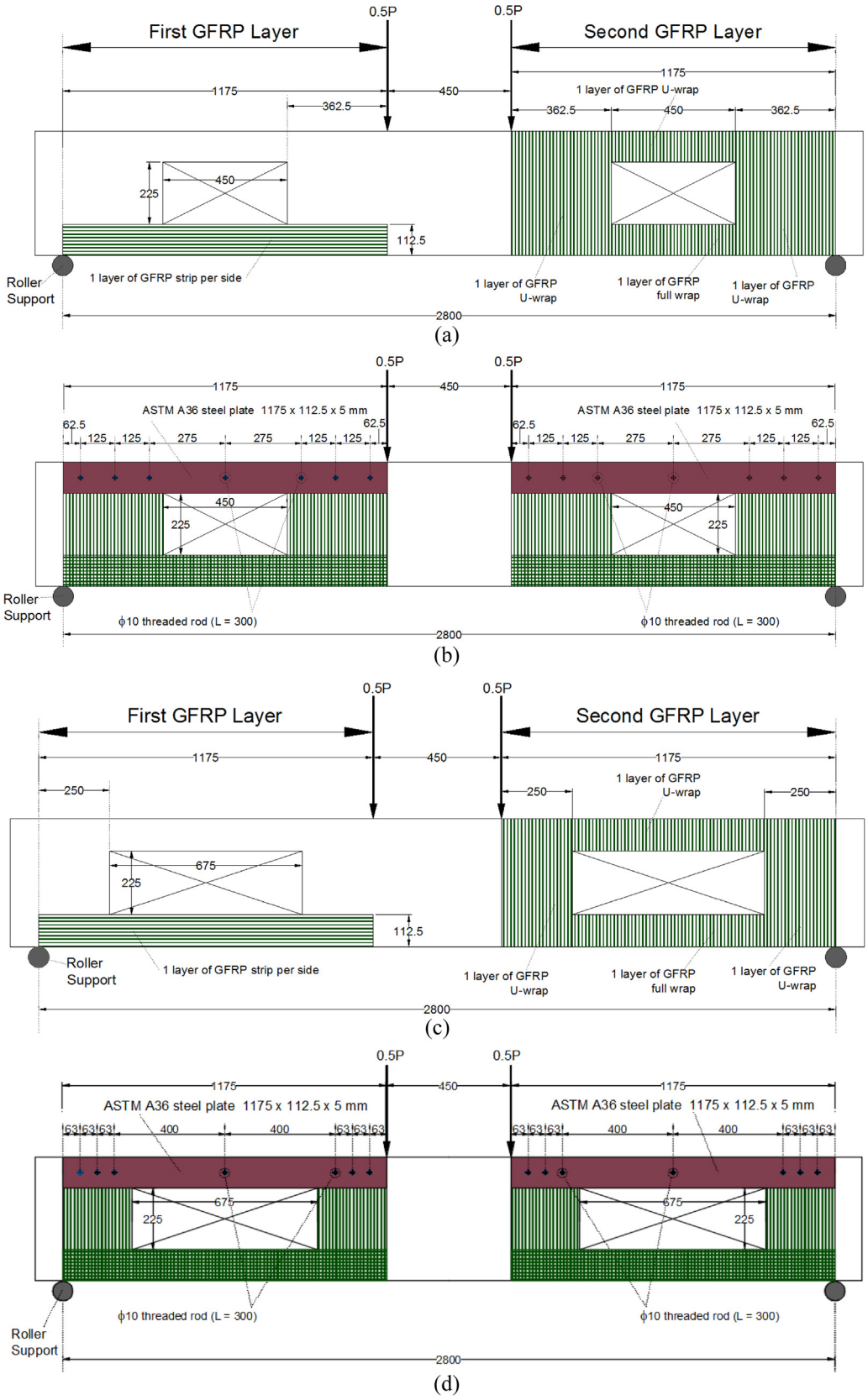

Fig. 5. Details of beams strengthened with scheme-2 (Note: All dimensions are in mm): (a) GFRP layers of specimen BS2-O1; (b) Steel plates of specimen BS2-O1; (c) GFRP layers of specimen BS2-O2; (d) Steel plates of specimen BS2-O2.

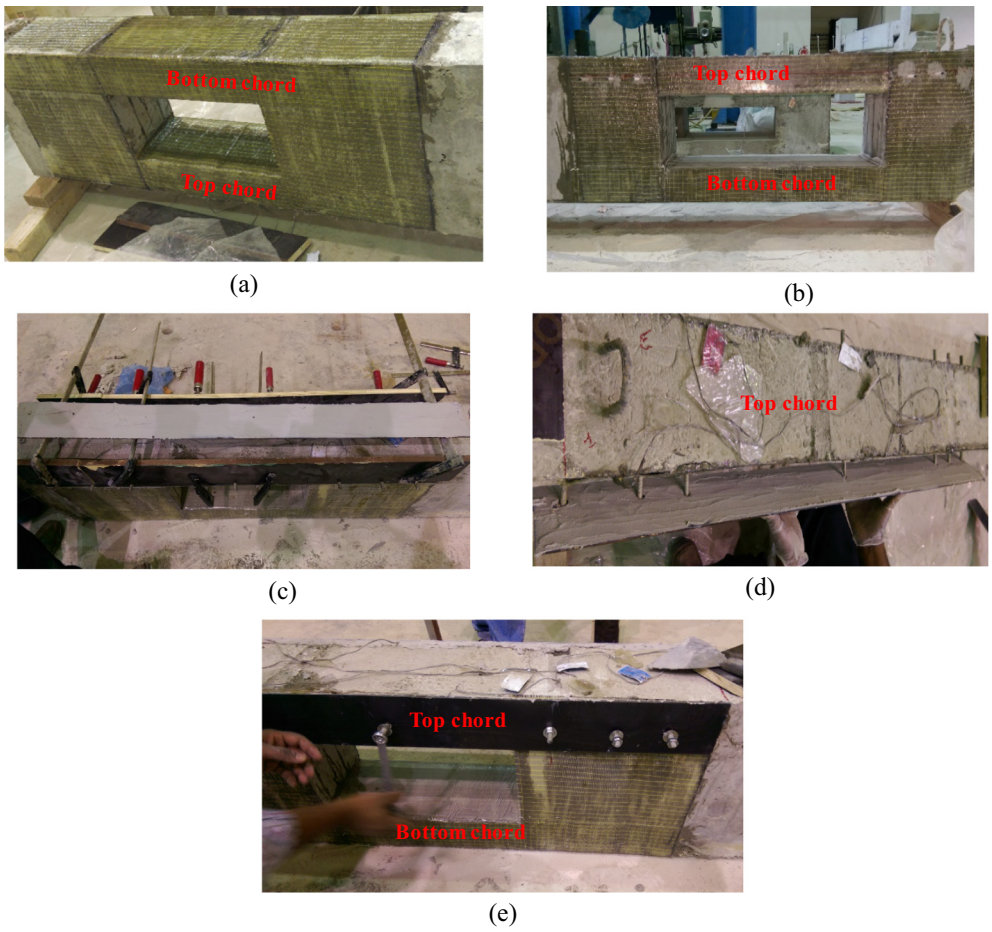

Fig. 6. Steps involved in strengthening of beams using scheme-2: (a) GFRP-strengthened beam; (b) Holes drilled and threaded rods passed; (c) Sika-41 epoxy applied to steel plates; (d) Steel plates passed through the rods; (e) Nuts being tightened.

Table 2
Material properties used in the FE modeling.

Concrete					
Material model	Type 159 (MAT_CSCM_CONCRETE)				
Density (kg/m^3)	2320				
Uniaxial compressive strength (MPa)	50				
Max aggregate size (mm)	10				
Steel rebars, threaded rods & plates	*ϕ8*	*ϕ10*	*ϕ16*	*Threaded rods*	*Plates*
Material model	Type 24 (MAT_PIECEWISE_LINEAR_PLASTICITY)				
Density (kg/m^3)	7850				
Young's modulus (GPa)	200				
Poisson's ratio	0.3				
Yield stress (MPa)	570	575	575	350	250
Tangent modulus (MPa)	0	982	982	0	0
Plastic strain to failure (%)	11.7	11.7	11.7	19.8	19.9
FRP material	*CFRP system*	*GFRP system*			
Material model	Type 54-55 (MAT_ENHANCED_COMPOSITE_DAMAGE)				
Density (kg/m^3)	1740	2550			
Thickness per layer (mm)	1.0	1.3			
Young's modulus in long. dir. (GPa)	82	20.9			
Young's modulus in transverse dir. (GPa)	3.6	0.9			
Longitudinal tensile strength (MPa)	834	460			
Transverse tensile strength (MPa)	83.4	46			

cut, machined and then tested as per ASTM A370 [27]. The average value of yield strength of steel plates is given in Table 2. Both CFRP and GFRP systems were unidirectional. They were applied onto the concrete surface using the conventional wet lay-up method. Tensile tests, as per ASTM D3039 [28], were conducted on the coupons of CFRP as well as GFRP sheets. Table 2 provides the results of the material testing.

2.4. Test setup and procedure

Fig. 7 shows the sensor locations and the test setup. The RC beams were tested under the application of two-point loads with a shear span of 1175 mm, as shown in Fig. 7. The AMSLER testing machine of 2000-kN capacity was used for applying the load with the help of a stiff steel beam. The load measurements during the exper-

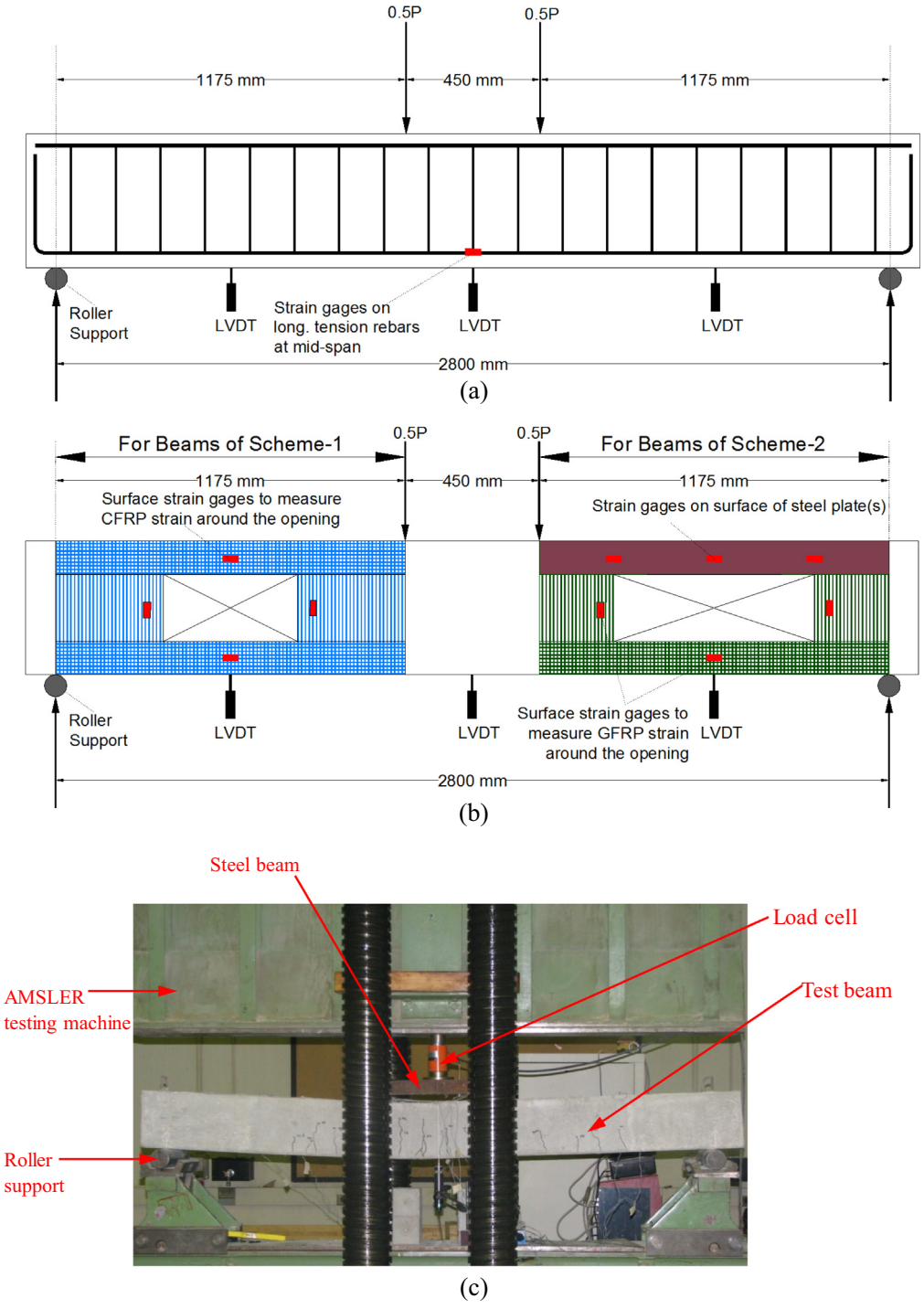

Fig. 7. Instrumentation layout and test setup: (a) Sensor locations for unstrengthened beams; (b) Sensor locations for strengthened beams; (c) Test setup.

iment were taken using the load cell. The RC beams were tested to failure under displacement-controlled condition at a loading rate of 1 mm/min. The deflection of beams was recorded with the help of Linear Variable Displacement Transducers (LVDTs). Moreover, strain gages were affixed to the steel rebars to record their strains during the test. Moreover, surface strain gages were bonded to the FRP sheets and steel plates to measure their strains around the opening, as seen in Fig. 7.

3. Test results and discussion

Table 3 presents the summary of test results of the seven specimens in terms of key parameters of load-deflection curves. It should be noted that the ultimate state used in Table 3 is defined as the state where the load drops by 20% of its peak value based on New Zealand Standard-1992 [29]. Table 4 displays peak strains for all of: beam bottom rebars at mid-span, first FRP layer at mid-length of top and bottom chords, second FRP layer at mid-depth of high-moment end, and steel plate at high-moment end of top chord. Fig. 8 shows the variation of load with mid-span deflection of the RC beam. Fig. 9 illustrates the final failure modes of tested beams.

As observed from Fig. 8, the control specimen BC-N with no opening revealed approximately the standard bilinear behavior of RC beams. Typical flexural failure was observed which started with

Table 3
Comparison of experimental and FE load-deflection characteristics for test beams.*

Beam ID	Results	P_y (kN)	P_u (kN)	Δ_y (mm)	Δ_u (mm)	K_s (kN/mm)	μΔ	E_u (kN·m)	Failure mode
BC-N	EXP	208	239	9.4	83.9	22.1	8.9	17.6	Y-CC
	FE	226	238	9.4	85.7	24.2	9.1	18.2	Y-CC
	EXP/FE	0.92	1.00	1.00	0.98	0.92	0.98	0.96	
BC-O1	EXP	NY	82	NY	11.4	7.3	–	0.6	SF
	FE	NY	83	NY	11.4	7.5	–	0.7	SF
	EXP/FE	–	0.99	–	1.00	0.98	–	0.94	
BS1-O1	EXP	NY	132	NY	18.2	8.8	–	1.4	DB-SF
	FE	NY	132	NY	16.2	9.7	–	1.5	DB-SF
	EXP/FE	–	1.00	–	1.12	0.91	–	0.97	
BS2-O1	EXP	212	236	16.5	38.6	12.9	2.3	7.1	Y-BKL-SF
	FE	222	231	17.7	39.3	12.5	2.2	7.1	Y-BKL-SF
	EXP/FE	0.96	1.02	0.93	0.98	1.03	1.06	1.01	
BC-O2	EXP	NY	69	NY	18.7	4.1	–	0.9	SF
	FE	NY	70	NY	18.4	3.9	–	0.8	SF
	EXP/FE	–	0.99	–	1.02	1.06	–	1.11	
BS1-O2	EXP	NY	113	NY	25.4	5.0		2.1	DB-SF
	FE	NY	112	NY	20.8	5.4		1.9	DB-SF
	EXP/FE	–	1.01	–	1.22	0.93		1.07	
BS2-O2	EXP	NY	166	NY	47.6	6.3	–	5.6	BKL-SF
	FE	NY	151	NY	43.6	5.7	–	4.9	BKL-SF
	EXP/FE	–	1.10	–	1.09	1.10	–	1.15	
Statistical parameters for EXP/FE	Mean	0.94	1.02	0.97	1.06	0.99	1.02	1.03	
	SD	0.03	0.04	0.05	0.09	0.07	0.06	0.08	
	CV (%)	3.01	3.81	5.13	8.46	7.56	5.55	7.87	
	Min.	0.92	0.99	0.93	0.98	0.91	0.98	0.94	
	Max.	0.96	1.10	1.00	1.22	1.10	1.06	1.15	

* P_y and Δ_y = load and mid-span deflection at yielding of main steel; P_u = ultimate load; Δ_u = mid-span deflection at ultimate state; K_s = effective pre-yield stiffness; μ_Δ = deflection ductility ratio = Δ_u/Δ_y; E_u = energy dissipated at ultimate state; Y-CC = steel yielding followed by concrete crushing at mid-span; SF = shear failure at opening; DB-SF = FRP debonding followed by shear failure at opening; Y-BKL-SF = steel yielding at mid-span followed by out-of-plane buckling of steel plates and finally shear failure at opening; BKL-SF = out-of-plane buckling of steel plates followed by shear failure at opening; NY = No steel yielding; SD = Standard deviation; CV = Coefficient of variation.

Table 4
Comparison of experimental and FE peak strains for test beams*

Beam ID	Results	Strain in bottom rebars at mid-span (με)**	Strain in first FRP layer (με)		Strain in second FRP layer at mid-depth of high-moment end (με)	Steel plate strain at high-moment end of top chord (με)**
			At mid-length of bottom chord	At mid-length of top chord		
BC-N	EXP	NA	–	–	–	–
	FE	***69,540***	–	–	–	–
	EXP/FE	–	–	–	–	–
BC-O1	EXP	957	–	–	–	–
	FE	961	–	–	–	–
	EXP/FE	1.00	–	–	–	–
BS1-O1	EXP	1822	660	1906	55	–
	FE	1742	602	2077	48	–
	EXP/FE	1.05	1.10	0.92	1.14	–
BS2-O1	EXP	***13,195***	NA	–	2510	***3855***
	FE	***13,956***	2521	–	2720	***3806***
	EXP/FE	0.95	–	–	0.92	1.01
BC-O2	EXP	667	–	–	–	–
	FE	718	–	–	–	–
	EXP/FE	0.93	–	–	–	–
BS1-O2	EXP	1671	1249	983	33	–
	FE	1412	1508	929	43	–
	EXP/FE	1.18	0.83	1.06	0.77	–
BS2-O2	EXP	2266	NA	–	16,362	***5953***
	FE	2120	1195	–	14,479	***5326***
	EXP/FE	1.07	–	–	1.13	1.12

* EXP = experimental; FE = finite element; NA = not available data.
** Values in italic bold font indicate steel yielding.

the yielding of the main tension rebars. The failure was initiated through the development of flexural cracks at the mid-span and the final failure was through concrete crushing in the maximum moment region (Fig. 9(a)). For unstrengthened beams with openings (BC-O1 and BC-O2), the increase in load caused diagonal shear cracks and the beams failed suddenly as a result of shear failure at the opening at the maximum loads of 82 and 69 kN for specimens BC-O1 and BC-O2, respectively. As seen from Fig. 9(b) and (c), major shear cracks appeared in both the chords (top and bottom) of the beam. The final failure of specimen BC-O1 was as a result of the top chord of the beam failing in shear, whereas, specimen BC-O2 failed by shear failure of the bottom chord. The test results revealed that as a result of the opening, the beam failure mode changed from flexure in solid beam BC-N to brittle shear failure in the beam with openings. There were hardly any noticeable flexural cracks in these beams.

As mentioned earlier, beams BS1-O1 and BS1-O2 were upgraded using two layers of unidirectional CFRP sheets and this

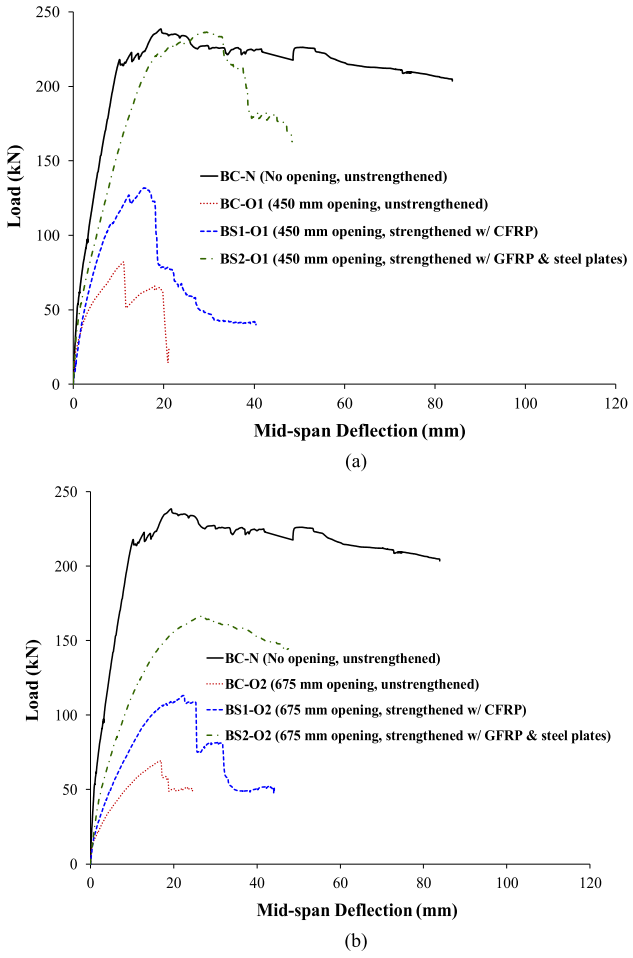

Fig. 8. Load-deflection curves for tested beams: (a) Beams with 450 mm opening; (b) Beams with 675 mm opening.

strengthening scheme was designed after observing the failure mode of the unstrengthened beams with openings BC-O1 and BC-O2. The purpose of the strengthening was to make sure the regions around the openings were enhanced so as to avoid shear failure, as far as possible, and to increase the ultimate load of the beam. Fig. 9(d) and (e) show the final failure mode for the strengthened beams BS1-O1 and BS1-O2. The test results, shown in Fig. 9, indicate that the final failure of the beams was through the shearing of the top chord above the opening. A diagonal shear crack was observed propagating from a small distance from the loading point all the way to the edge of the opening thereby causing shear failure of the top chord. However, before the final failure, debonding of the CFRP sheets wrapping the top chord at the same location of the massive shear crack was noticed. Peak loads were 132 kN and 113 kN for specimens BS1-O1 and BS1-O2, respectively. As seen in Table 3, these peak loads were significantly less than even the yield load of control beam BC-N and as presented in Table 4, the peak recorded steel strains at mid-span were about 63% and 58% of the rebar yield strain for beams BS1-O1 and BS1-O2, respectively.

As detailed earlier, scheme-2 involved using two layers of GFRP sheets along with steel plates for anchoring the GFRP sheets to the concrete surface and to add shear strength to the top chord. The anchorage system was developed as a way to avoid debonding failure of the FRP laminates, which was observed in the beams strengthened with scheme-1. For beam BS2-O1 strengthened with scheme-2, the peak load was 236 kN, which is almost same as that for control solid beam BC-N. This demonstrates the effectiveness of the strengthening scheme-2 for beam with openings of 450 mm length. For this beam, main tension steel at mid-span yielded as seen in Tables 3 and 4. Due to steel yielding, flexural cracks were observed in the maximum moment zone and the beam went into the inelastic stage and continued to carry more deformation until the steel plates were found to buckle at the location of the interface between the top chord and the edge of the opening (Fig. 9(f)) indicating its involvement in resisting shear forces at that location. Subsequently, sudden shear failure occurred in the top chord and the load dropped suddenly at a deflection of about 33 mm (see Fig. 8(a)). However, for specimen BS2-O2 with larger opening of 675 mm length and strengthened with scheme-2, main tension steel did not yield and peak load was 166 kN (about 80% of the yield load of solid beam BC-N). The failure of this beam was due to the buckling of steel plates close to the edge of the opening (see Fig. 9(g)) followed by shear failure in the top chord.

Fig. 10 shows the influence of the strengthening scheme on performance of test beams with respect to both peak load and effective stiffness. It is clear that the FRP strengthening is relatively more efficient in increasing the load carrying capacity of the RC beams than enhancing the effective pre-yield stiffness and its usefulness reduces with the increase in the opening size. It is also evident that the strengthening scheme-2 is superior to scheme-1 for the two opening sizes. For 450 mm opening, the reduction in peak load due to opening decreased from 45% in case of scheme-1 to 1% in case of scheme-2. However, and as seen in Fig. 10(a) for 675 mm opening, loss in peak load due to opening was reduced from 53% in case of scheme-1 to 30% in case of scheme-2. As seen in Fig. 10(b), the strengthening schemes were less efficient in reducing the loss in effective stiffness. For 450 mm opening, loss in stiffness was reduced from 60% in case of scheme-1 to 42% in case of scheme-2; however, for 675 mm opening, loss of stiffness due to opening was slightly reduced from 77% in case of scheme-1 to 72% in case of scheme-2 (Fig. 10(b)).

4. Finite element modeling

The finite element modeling of the tested beams was done using a general-purpose FE software LS-DYNA [24]. The model was created using the general-purpose package FEMB PC Pre-Processor 28.0. Taking advantage of the symmetry, half length of the beam was only modeled.

4.1. Geometry and FE mesh

The FE mesh of specimens BC-N and BC-O1 is shown in Fig. 11 (a) and (c). The concrete was meshed using eight-node solid hexahedron elements of reduced integration. The FE model of steel reinforcement of specimens BC-N and BC-O1 is displayed in Fig. 11(b) and (d). The 2-node Hughes-Liu beam elements were used to model the steel rebars and stirrups of RC beams, whereas, 4-node Belytschko-Tsay shell elements [30] were used to model FRP laminates of strengthened specimens, as shown in Fig. 11(e) and (f). Eight-node reduced integration solid elements and 2-node Hughes-Liu beam elements, respectively, were employed to model steel plates and threaded rods for beams BS2-O1 and BS2-O2 as seen in Fig. 11(g). Size of elements used in the FE mesh varied from 3 to 25 mm. The numerical convergence was investigated and it was found that further refinement of finite element mesh could have little effect on the numerical output; however, this may noticeably increase the computation time of analysis. Perfect bond was assumed between rebars and the surrounding concrete. The bond between the steel plates and the FRP laminates was also assumed as perfect.

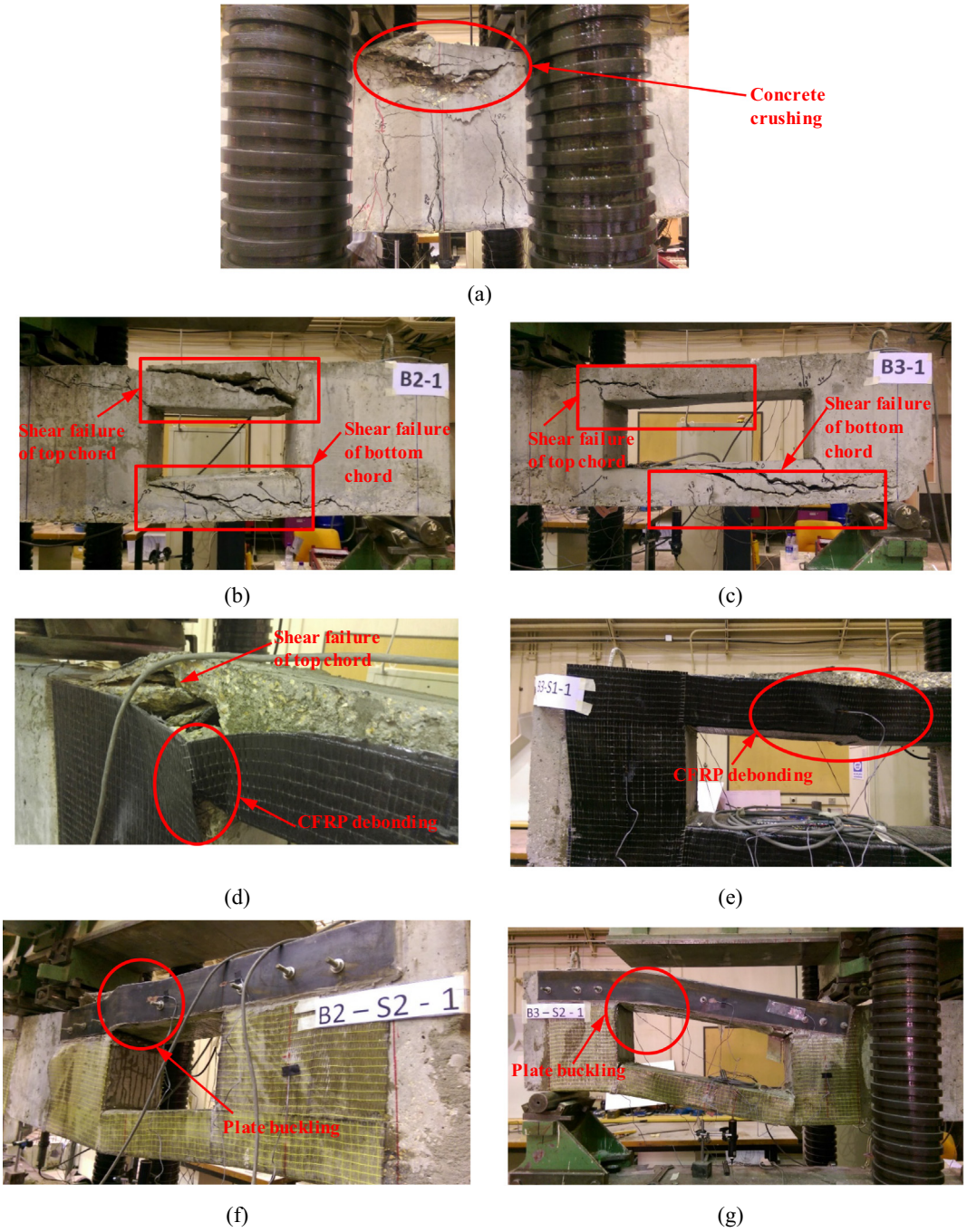

Fig. 9. Mode of failure for: (a) BC-N; (b) BC-O1; (c) BC-O2; (d) BS1-O1; (e) BS1-O2; (f) BS2-O1; (g) BS2-O2.

4.2. Constitutive models

The material model type 159, MAT_CSCM_CONCRETE was employed to model the concrete volume. This is a smooth or continuous cap model available in LS-DYNA for solid elements, with a smooth intersection between the shear yield surface and the hardening cap as shown in Fig. 12. In this model, the initial damage surface coincides with the yield surface. Fig. 12 shows the general shape of concrete model yield surface in two dimensions. The yield surface is formulated in terms of three stress invariants. The model uses the J_1-the first invariant of the stress tensor and two invariants of deviatoric stress tensor, namely, J'_2 and J'_3. The three-invariant yield function is based on these three invariants, and the cap hardening parameter, K as shown in Eq. (1).

$$f\left(J_1, J_2^{'}, J_3^{'}, K\right) = J_2^{'} - R^2 F_f^2 F_c \tag{1}$$

where F_c is the hardening cap, F_f is the shear failure surface, and R is the Rubin three-invariant reduction factor. The cap hardening parameter, K, is the value of the pressure invariant at the intersection of the cap and shear surfaces. For the shear failure surface, the strength of concrete is modeled by the shear surface in the tensile and low confining pressure regimes. The shear surface F_f is defined along the compression meridian as shown in Eq. (2).

$$F_f(J_1) = \alpha - \lambda exp^{-\beta J_1} + \theta J_1 \tag{2}$$

where the values of α, β, λ and θ are obtained by fitting the model surface to strength measurements from tests conducted on plain concrete.

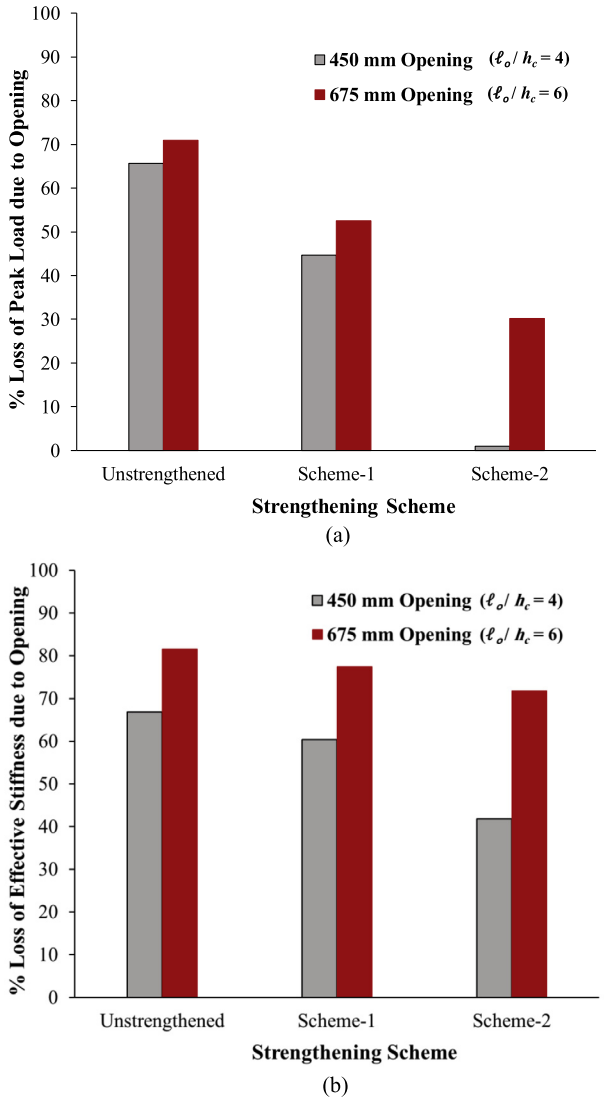

Fig. 10. Effect of strengthening scheme on performance of tested beams: (a) with respect to peak load; (b) with respect to effective stiffness.

The cap is used to model plastic volume change related to pore collapse, which is not explicitly modeled. The initial location of the cap determines the onset of plasticity in isotropic compression and uniaxial strain. The elliptical shape of the cap allows the onset for isotropic compression to be greater than the onset for uniaxial strain, in agreement with shear enhanced compaction data. Without ellipticity, a "flat" cap would produce identical onsets. The motion of the cap determines the shape (hardening) of the pressure-volumetric strain curves via fits with data. Without cap motion, the pressure-volumetric strain curves would be perfectly plastic. Rate effects are modeled with viscoplasticity. Concrete cracking is considered using the traditional smeared crack approach. More details of this material model can be found in references [31,32]. In this material model, elements of concrete were allowed to erode when the maximum principal strain reached 0.05 [32].

The steel rebars, plates and threaded rods were modeled using material type 24, MAT_PIECEWISE_ LINEAR_PLASTICITY. This material is suited to model elasto-plastic materials with an arbitrary stress versus strain curve and an arbitrary strain rate dependency. It is available for beam, shell and solid elements. In order to model the FRP sheets, the material model type 54-55, MAT_ENHANCED_-COMPOSITE_DAMAGE was employed. An orthotropic material with optional brittle failure can be defined using this material card. Three failure criteria are possible for this card and the one proposed by Chang and Chang [33] was utilized in this study. A summary of the material properties used in this study is presented in Table 2.

4.3. Contact modeling

The tiebreak surface-to-surface contact of LS-DYNA was used to model the bond between FRP sheets and concrete. In this case, concrete surface was taken as master and the FRP surface was input as slave as seen in Fig. 13(a). Tiebreak contact is a special type of contact and it works the same as common contact types under compressive load. Under the action of shear and tensile forces, the tiebreak permits the disengagement of the tied contact surfaces based on the bond strength failure criterion:

$$\left(\frac{|\sigma_n|}{NFLS}\right)^2 + \left(\frac{|\sigma_s|}{SFLS}\right)^2 \geq 1 \tag{3}$$

where σ_n and σ_s are the normal and shear stresses, respectively. However, *NFLS* and *SFLS* are the normal and shear failure stresses, respectively, given by [34,35]:

$$NFLS = 0.62\sqrt{f'_c} \quad (MPa) \tag{4}$$

$$SFLS = 1.5\beta_w NFLS \tag{5}$$

where f'_c is the compressive strength of concrete and β_w is a parameter given by

$$\beta_w = \sqrt{\frac{2.25 - b_f/b_c}{1.25 + b_f/b_c}} \tag{6}$$

where b_c is the width of RC beam, and b_f is the width of FRP sheet. A schematic sketch of Eq. (3) is presented in Fig. 13(b). After failure, this contact type behaves as a surface-to-surface contact with no thickness offsets. In addition, after failure, no interface tension is possible. It is worth mentioning here that the contact model used in this study has been validated in earlier studies [13,36,37].

4.4. Boundary conditions and loading

Taking advantage of the symmetry in the test specimens, only half of the RC beam was used in the numerical modeling. The nodes lying on the plane of symmetry were restrained against rotation about the global Y- and Z-axes and displacement along global X-axis. Nodes at location of beam support were restrained against displacement in the global Z-axis. A node set was used for applying the displacement controlled loading along Z-direction during the test.

4.5. Loading strategy

LS-DYNA uses explicit time integration algorithms for solving the problems. The load application process in LS-DYNA is time-history dependent. Since the testing procedure involved displacement controlled static loading, a constant velocity was assigned to the displacement controlled node set. In order to reduce the solution time, the rate of change of displacement was defined as 10 mm/s which could represent quasi static dynamic loading. The inertia force developed in this case is considered marginal and would not affect the results of the FE modeling. In addition, strain rate effects associated with the dynamic analysis were turned off in the material models.

5. Validation of numerical modeling and analysis

Test results of the seven test specimens were used for the validation of the FE modeling. The results of the FE analysis are discussed in the subsequent sub-sections.

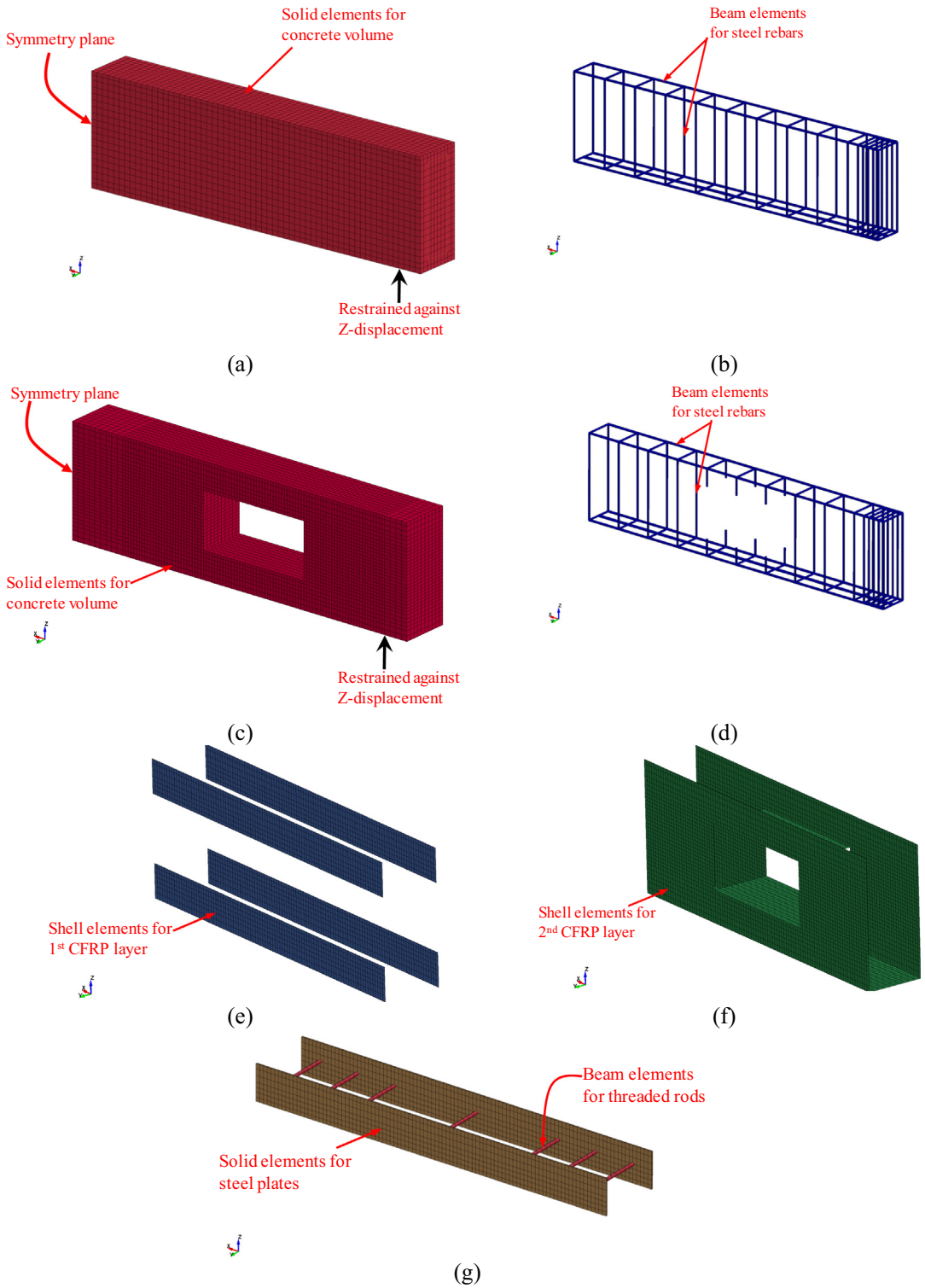

Fig. 11. FE model for one-half of specimens: (a) Concrete volume for beam BC-N; (b) Steel rebars for beam BC-N; (c) Concrete volume for beam BC-O1; (d) Steel rebars for beam BC-O1; (e) 1st CFRP layer for beam BS1-O1; (f) 2nd CFRP layer for beam BS1-O1; (g) Steel plates with rods for beam BS2-O1.

5.1. Modes of failure

Fig. 14 displays the modes of failure for some of the tested beams, obtained using the LS-DYNA's post-processing software (LS-PrePost) at the end of the analysis time. The modes of failure in this figure are shown using contours of maximum principal strains at the mid-surface. It is noticed from this figure that the modes of failure observed in the results of numerical analysis are either similar or almost identical to the ones determined experimentally. The results of analysis revealed that the failure of control test specimen BC-N with no opening started with the development of the flexural cracks and the beam ultimately failed by crushing of concrete, as illustrated in Fig. 14(a). For unstrengthened beams with web openings (BC-O1 and BC-O2), sudden shear failure occurred in the top and bottom chords of the RC beam, as seen in Fig. 14(b) and (c). No flexural cracks were observed in the

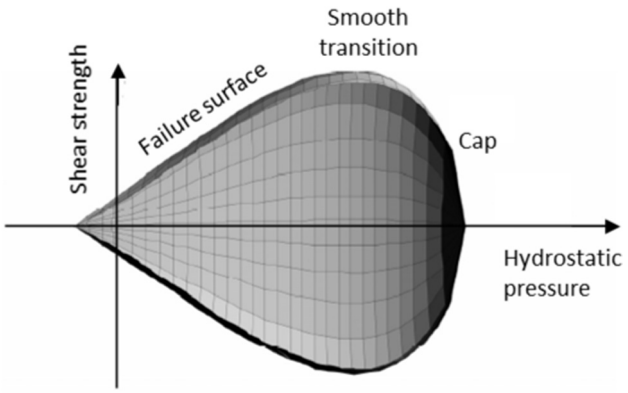

Fig. 12. General shape of the concrete model yield surface in two-dimensions.

maximum-moment region of specimens BC-O1 and BC-O2, as depicted from Fig. 14(b) and (c), which agrees well with the test results discussed earlier. Fig. 14(d) displays the FE mode of failure for strengthened beam BS1-O1. As observed from the figure, shear failure occurred in the top chord above the opening and it was preceded by debonding of the CFRP laminates wrapping the top chord. Similar to test observations, noticeable flexural cracks did not develop in the maximum-moment region and as seen in Fig. 14(d), limited erosion occurred in the concrete cover below the main tension steel rebars. Presented in Fig. 14(e) is the FE mode of failure for specimen BS2-O2 with opening of 675 mm length and strengthened with scheme-2. Similar to the experimental observations, failure of this beam was because of the out-of-plane buckling of steel plates and ultimately by shear failure in the top chord above the opening. Flexural cracks were not observed in the maximum-moment region, as seen from Fig. 14(e).

5.2. Load-deflection response

Fig. 15 depicts a comparison between the experimental and numerical variation of applied load versus mid-span deflection of RC beams for the seven tested specimens. The figure shows good agreement between the numerical and experimental load–deflection curves and especially the peak loads for all test specimens. Table 3 enlists the comparison details in terms of load-deflection characteristics in addition to statistical parameters of the experimental-to-predicted ratios in terms of mean, standard deviation, coefficient of variation and minimum and maximum values. As seen from Table 3, the numerical mid-span deflection at yield and ultimate loads deviated from experiments by 0%–7% and 0%–22%, respectively. However, the numerical results of yield

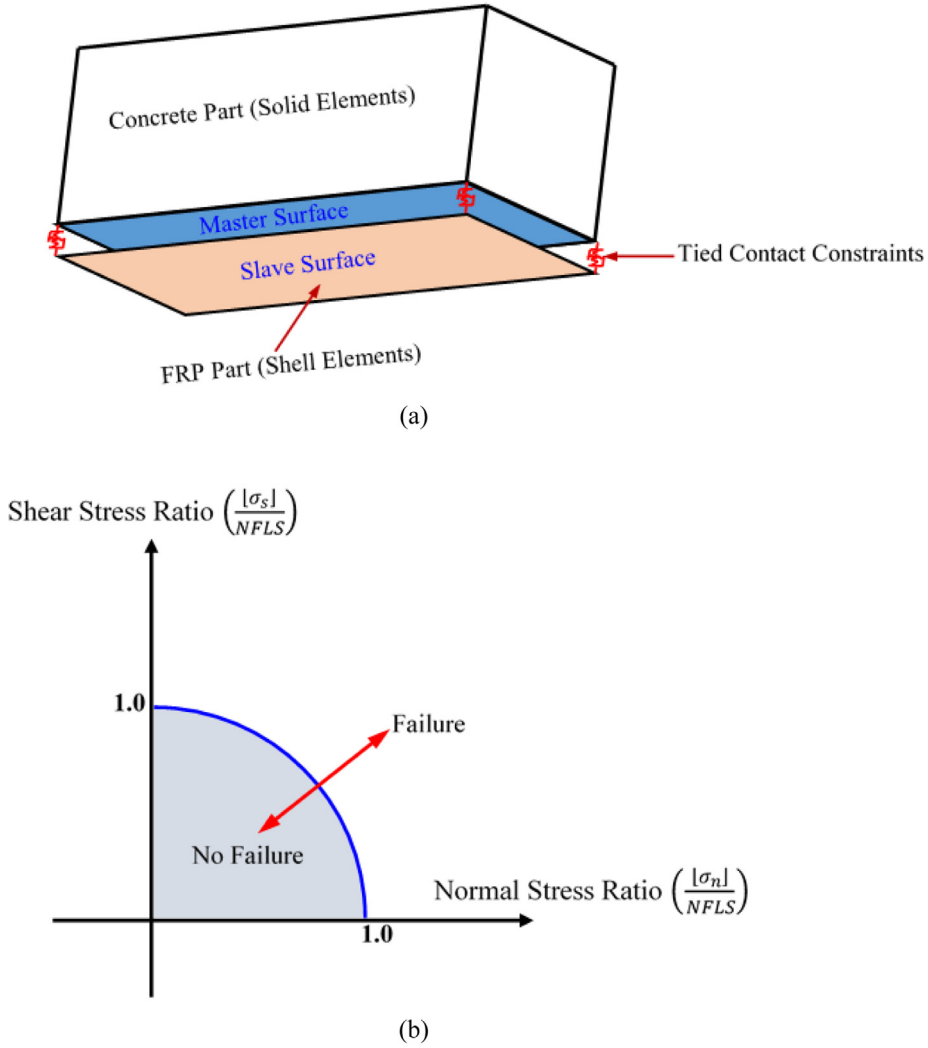

Fig. 13. Tiebreak surface-to-surface contact of LS-DYNA: (a) Master and slave surfaces; (b) Schematic sketch of bond strength failure criterion.

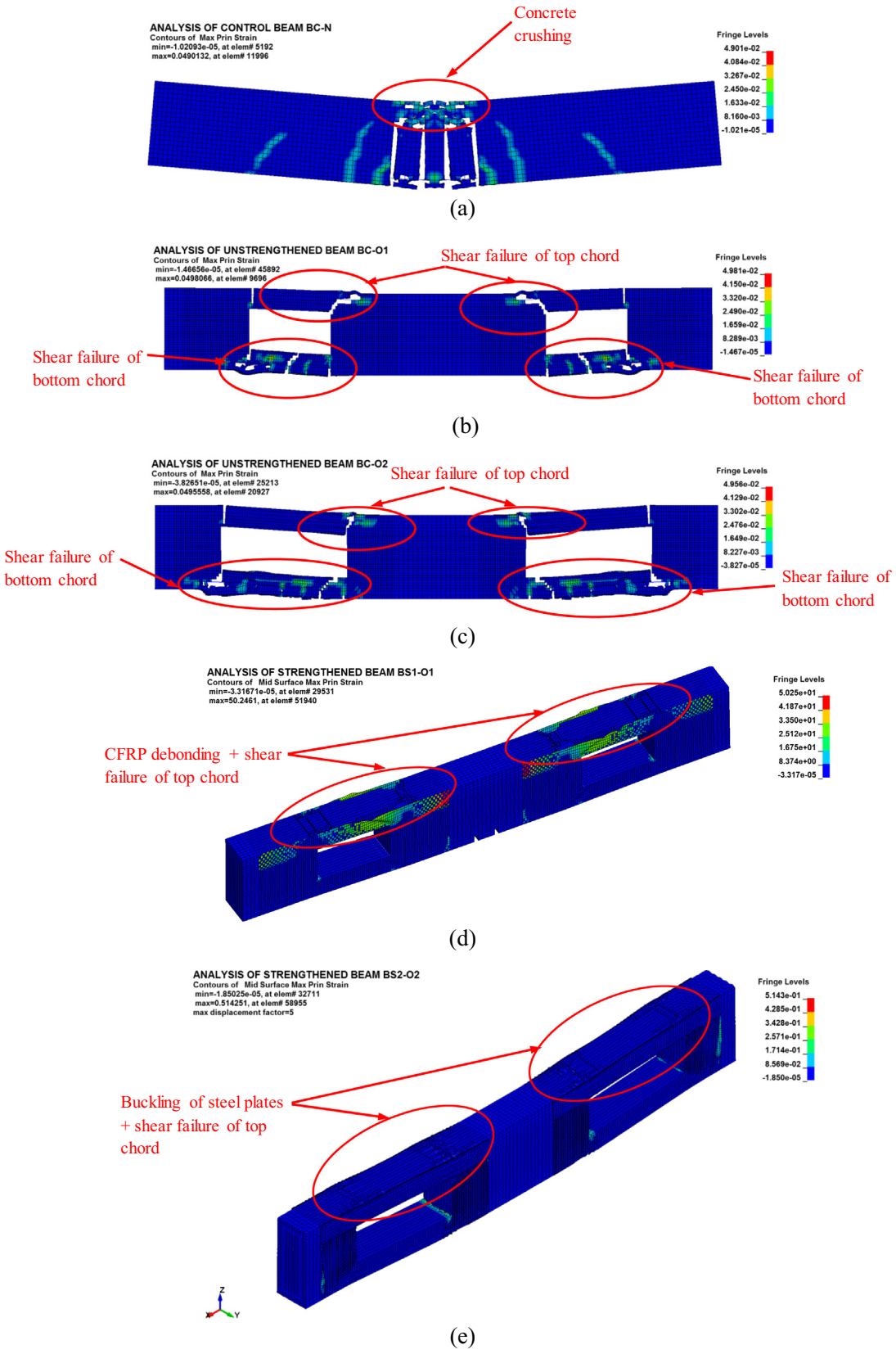

Fig. 14. FE modes of failure for: (a) BC-N; (b) BC-O1; (c) BC-O2; (d) BS1-O1; (e) BS2-O2.

and peak loads were relatively better with the deviation for the two loads varying from 4%–8% and 0%–10%, respectively. Whereas, a deviation of 2%–6% was observed for deflection ductility. The effective stiffness of the beams was also well predicted by the numerical analysis with deviation ranging from 2% to 10%. As seen from Table 3, the prediction of energy dissipated at ultimate load

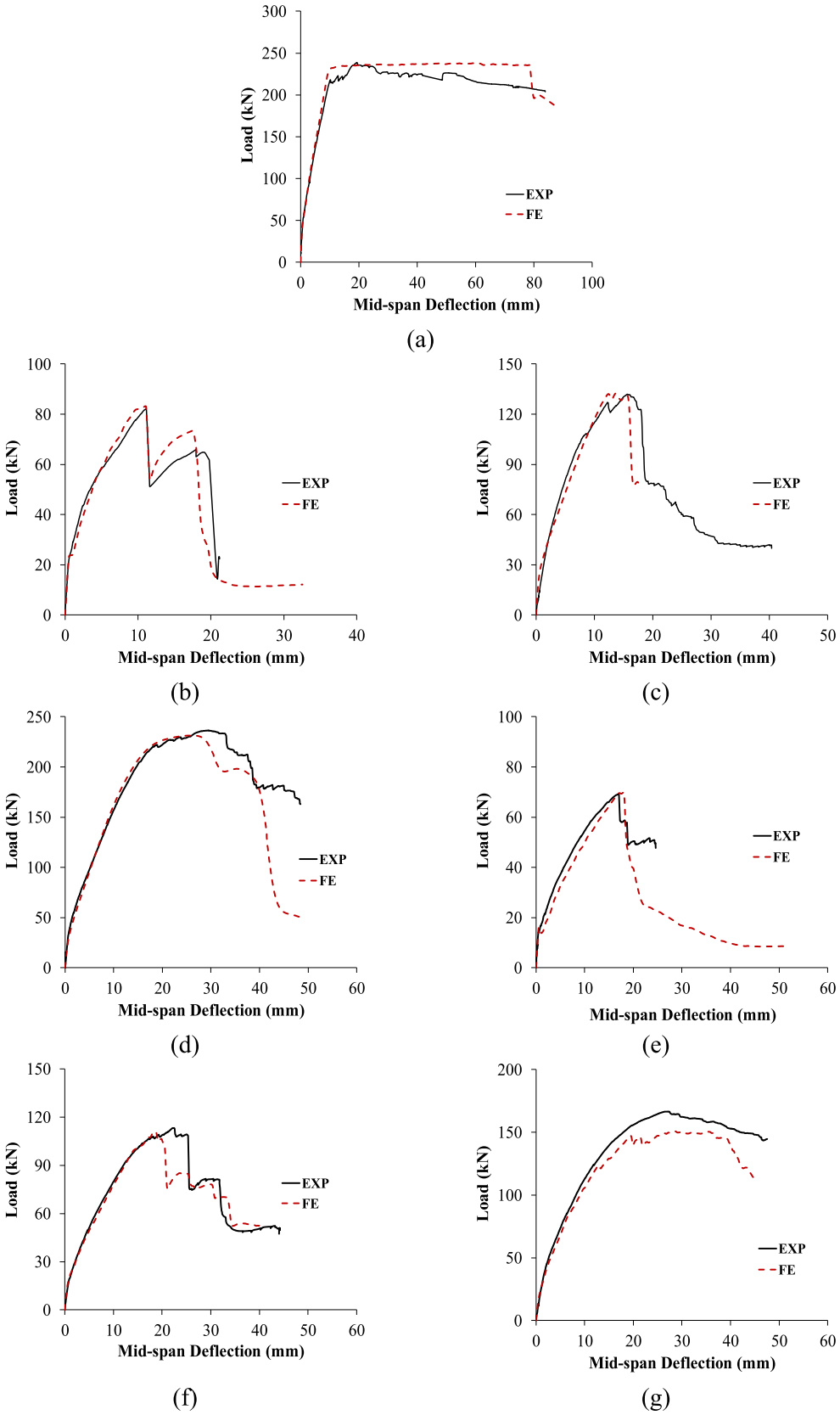

Fig. 15. Load-deflection comparison for: (a) BC-N; (b) BC-O1; (c) BS1-O1; (d) BS2-O1; (e) BC-O2; (f) BS1-O2; (g) BS2-O2.

was sufficiently close to the experimental values with the deviation ranging from 1% to 15%. Fig. 15 clearly shows that the numerical modeling and analysis procedures were successful at simulating the softening, which establishes the precision of the material modeling. The numerical analysis demonstrates the effectiveness of employing externally bonded FRP laminates in enhanc-

ing the load carrying capacity of RC beams with openings in shear zones. The numerical analysis also illustrated the superiority of strengthening scheme-2 over scheme-1 in terms of enhancing the load-deflection characteristics of RC beams with openings. Based on the FE analysis results, compared to the unstrengthened beams with openings, strengthening was successful in increasing the peak load by about 59% to 178% and 60% to 116% for beams with 450 mm and 675 mm openings, respectively.

5.3. Strain gage results

Presented in Table 4 are measured and predicted peak strains for all of: beam bottom rebars at mid-span, first FRP layer at mid-length of top and bottom chords, second FRP layer at mid-depth of high-moment end, and steel plate at high-moment end of the top chord. The predicted values are in good agreement with the experimental values. It is noted from Table 4 that due to CFRP debonding at the top chord of beams BS1-O1 and BS1-O2, horizontal FRP strains in the top chord ranging from about 10% to 20% of CFRP rupture strain were observed. Table 4 evidences the importance of using second GFRP layer (with fibers oriented vertically), in resisting shear stresses, especially at the high-moment end of the large opening of 675 mm length. High strains of about 74% and 64% of the GFRP rupture strain were measured and predicted, respectively, at such location as seen from Table 4 for specimen BS2-O2. For 450 mm opening, smaller shear stresses were induced at opening edge and as a result, smaller strains (about 12% of GFRP rupture strain) were observed in the second GFRP layer, as depicted from Table 4. Fig. 16 displays comparison curves of experimental and FE load versus strain of bottom rebars at mid-span of

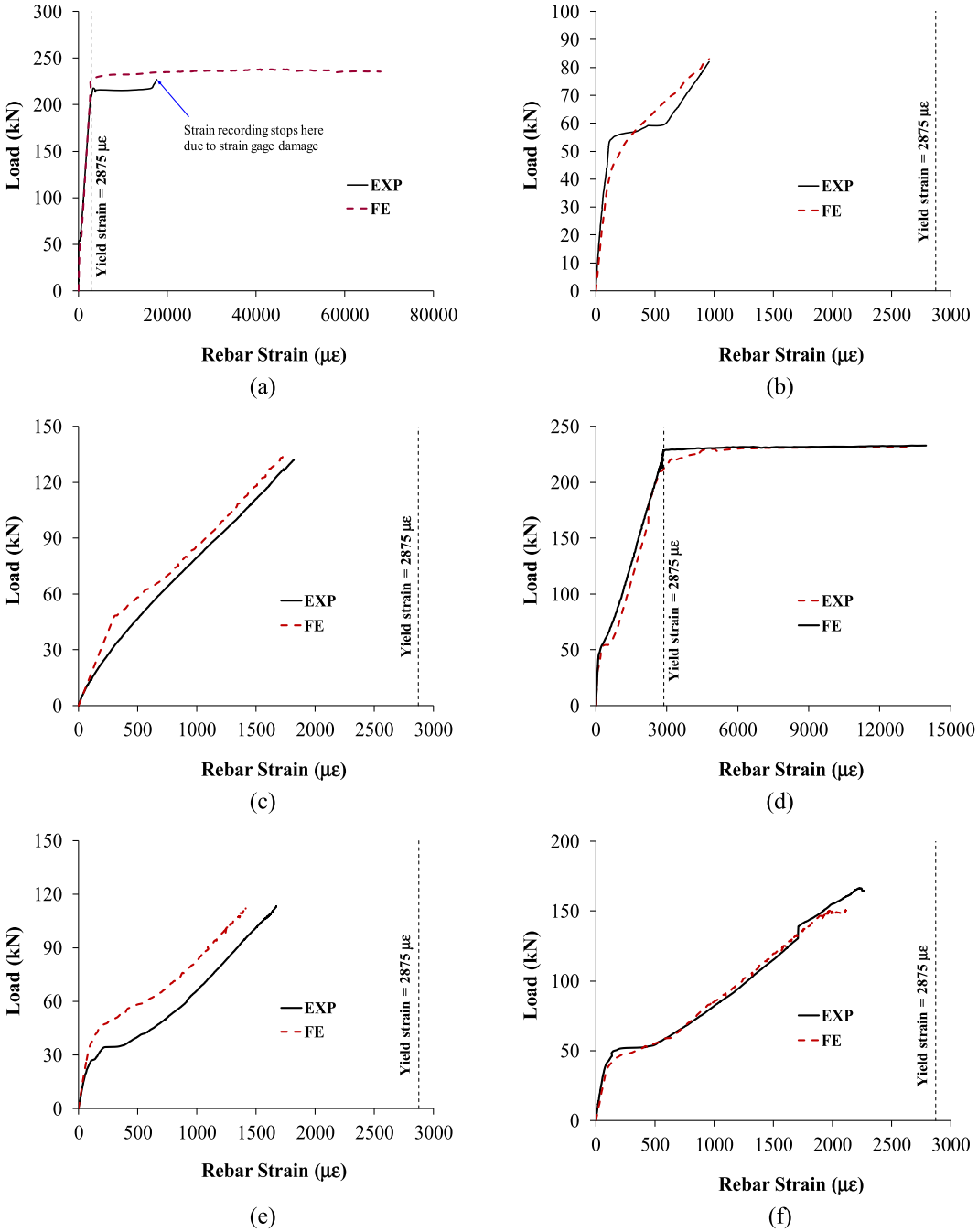

Fig. 16. Comparison curves of experimental and FE load vs. strain of bottom rebars at mid-span of: (a) BC-N; (b) BC-O1; (c) BS1-O1; (d) BS2-O1; (e) BS1-O2; (f) BS2-O2.

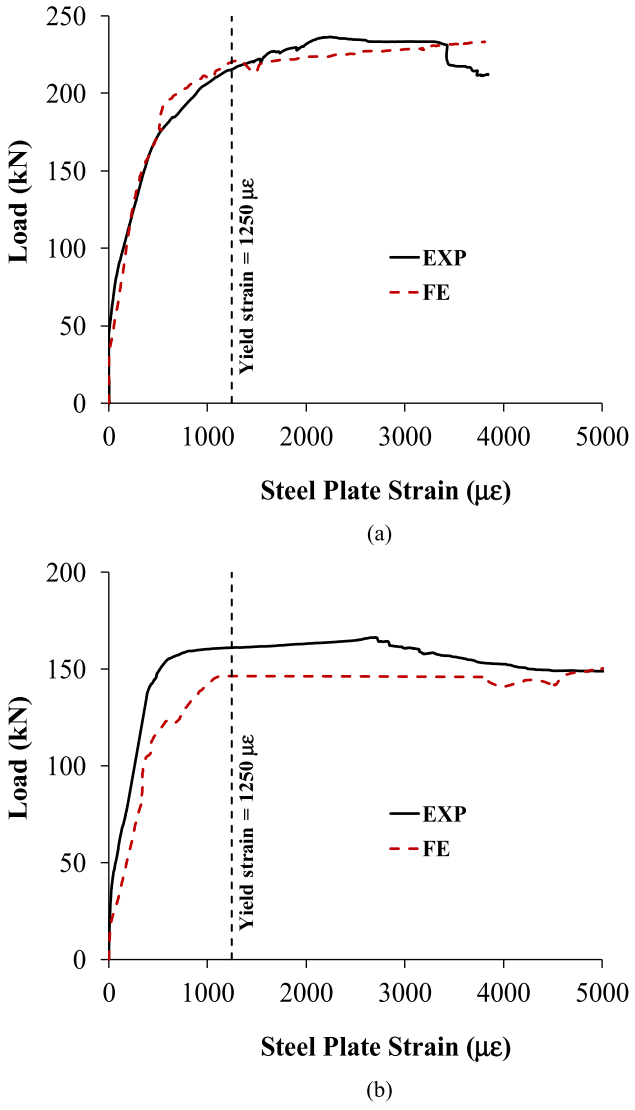

Fig. 17. Comparison curves of experimental and FE load vs. steel plate strain at edge of opening for: (a) BS2-O1; (b) BS2-O2.

representative test beams. It is evident that the control beam BC-N had a high ductility, which is typical for slender RC beams with under-reinforced sections. Fig. 16 reveals the effectiveness of strengthening scheme-2 in altering the behavior of unstrengthened specimen BC-O1 from brittle shear without steel yielding, as seen in Fig. 16(b), to ductile with strain ductility (ratio of peak rebar strain to its yield strain) of about 4.9, as seen in Fig. 16(d) for specimen BS2-O1. Fig. 17 presents comparison curves of experimental and FE load versus steel plate strain at edge of opening for strengthened beams BS2-O1 and BS2-O2. The figure shows that the predicted curves are in good agreement with the experimental curves. Fig. 17 demonstrated the full utilization of the yield capacity of the steel plates before buckling occurrence because strains as high as 3.0 and 4.8 times the yield strain were noticed for steel plates of specimens BS2-O1 and BS2-O2, respectively.

6. Parametric study

6.1. Effect of steel plate parameters

For simplicity of calculations, Euler buckling was assumed for steel plates as they may behave as columns under axial compression. Since a single row of threaded rods was used to tie the steel plates to the top chord, it may be conservatively assumed that the portion of the steel plate between rods might behave as a pinned-pinned column. Hence, the maximum pitch of threaded rods that could preclude elastic buckling of steel plates can be estimated approximately by equating the Euler stress to the yield strength of the steel plate:

$$s_{\max} = \pi t_p \sqrt{\frac{E_s}{12 f_{yp}}} \tag{7}$$

where t_p = thickness of steel plate; E_s = Young's modulus of steel = 2×10^5 MPa; f_{yp} = yield strength of steel plates. It is worth mentioning here that the above equation gives approximate value of spacing for shallow depth of top chord requiring only single row of anchor rods. However, for deeper top chords requiring two or more rows of anchors, Eq. (7) would require further improvement. For the 5 mm thick steel plates used in this study, $s_{\max}$ was calculated to be 128 mm. However, as seen in Fig. 5, maximum spacing of 275 and 400 mm was used for specimens BS2-O1 and BS2-O2, respectively, which exceeded the value (i.e. 128 mm) calculated from Eq. (7). Therefore, buckling occurred for plates of specimens BS2-O1 and BS2-O2. This buckling was followed by brittle shear failure in the top chord above the opening. In brief, plate buckling could have been mitigated by the use of either lesser rod spacing (not exceeding 128 mm) or plates with larger thickness. The validated FE modeling was used to investigate the effect of steel plate parameters on the behavior of strengthened RC beams with web openings in shear zones. In this regard, two new strengthening schemes (scheme-3 and scheme-4) were numerically investigated. Details of proposed schemes are shown in Fig. 18. It is clear that scheme-3 is the same as scheme-2 but with reduced maximum spacing of 125 mm between the rods, as seen in Fig. 18. As depicted from Fig. 18, strengthening scheme-4 is the same as scheme-2 but with a larger plate thickness of 6.0 mm and reduced rod spacing (maximum spacing of 138 mm was used). Four new specimens (BS3-O1, BS4-O1, BS3-O2 and BS4-O2) were added to the analysis matrix as seen in Table 5. The FE results of these specimens are summarized in Table 5. It is clear that proposed schemes 3 and 4 were successful in prohibiting the unwanted buckling of steel plates and the failure was a result of shear failure in the top chord above the opening that occurred at higher deformation levels. It is generally noted that scheme-4 was the best among all schemes in terms of enhancing the load-deflection characteristics of RC beams with openings. This could be due to the use of larger plate thickness of 6.0 mm, which added not only more confinement to the top chord concrete (it was accounted for in the adopted concrete model), but also more shear strength at opening location, which in the end delayed the onset of brittle shear failure. Fig. 19 shows load-deflection comparison curves of beams with 450 mm opening and strengthened with schemes 2, 3 and 4. It is clear from Table 5 and Fig. 19 that for beams with 450 mm opening, both schemes 3 and 4 enhanced the load-deflection characteristics of the beam over that of scheme-2. Compared to scheme-2, schemes 3 and 4, respectively, increased the peak load by about 1.7% and 2.2%, the deflection ductility by about 18% and 36% and the effective stiffness by about 5.6% and 10.4%. Also, schemes 3 and 4, respectively, enhanced the dissipated energy by about 17% and 34%, compared to scheme-2. Schemes 3 and 4 have also a remarkable effect on the strain ductility of specimen as it was noticeably increased by about 120% and 160% compared to scheme-2. For beams with 675 mm opening, schemes 3 and 4 also enhanced the load-deflection characteristics over that of scheme-2 (Table 5). Compared to scheme-2, strengthening schemes 3 and 4 enhanced the peak load by about 2.6% and 9.9%, respectively, and the effective stiffness by about 17.5% and 29.8%, respectively.

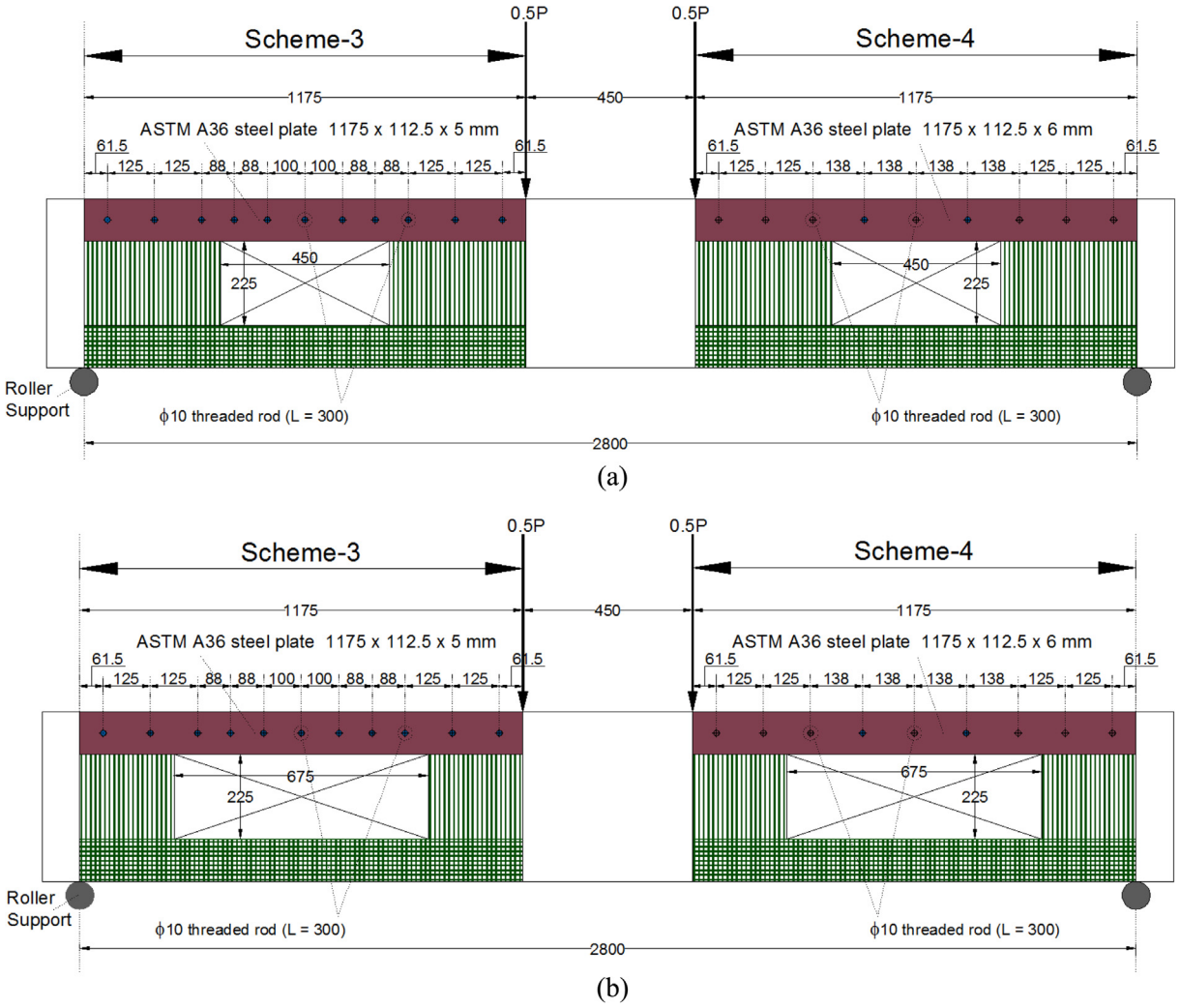

Fig. 18. Details of proposed strengthening schemes for beams with: (a) 450 mm opening; (b) 675 mm opening (Note: All dimensions are in mm).

6.2. Effect of opening size

The validated numerical modeling procedure, detailed previously, was extended to study the influence of different opening sizes on behavior of unstrengthened and strengthened beams having web openings in shear zones. Mansur and Tan [38] suggested criteria for deciding appropriate location of openings in RC beams. They recommended that the depth of web openings should not be more than 50% of the overall depth of the beam. Accordingly, in this study, the depth of the opening was not taken as a studied parameter and it was hence set equal to 225 mm. Mansur and Tan [38] also recommended that the distance of the openings from the supports should not be less than 50% of overall beam depth. The length of the opening was taken as a studied parameter and it was varied from zero (case of no opening) to 725 mm. The maximum opening length of 725 mm was chosen to comply with Mansur and Tan's recommendation as it corresponds to a distance of 225 mm (= 0.5 h) from the edge of the opening to the centerline of the support. Details of numerically investigated beams with different opening sizes are shown in Table 5. Sixteen opening lengths with ℓ_o/h_c (see Fig. 1) ranging from zero to 6.44 were numerically studied for unstrengthened beams. However, nine opening lengths with ℓ_o/h_c ranging from 2.0 to 6.44 were numerically investigated for strengthened beams as seen in Table 5. Since scheme-4 was previously found to give the best performance in terms of load–deflection characteristics, it was used in this parametric study. The results of FE analysis of RC beams with different opening sizes are given in Table 5.

Fig. 20 depicts the effect of opening size on load-deflection curves of unstrengthened beams. As seen from Table 5 and Fig. 20, it is clear that as the opening size increases, peak load, effective stiffness, deflection ductility and dissipated energy are reduced. Flexural failure was noticed for unstrengthened beams with $\ell_o/h_c \leq 1.0$; however, yielding of main tension steel was predicted for unstrengthened specimens with $\ell_o/h_c \leq 1.33$. In order to classify the web openings based on their size in terms of ℓ_o/h_c ratio as given by Mansur [2], the percentage losses of peak load and effective stiffness due to the opening were calculated for all unstrengthened specimens and plotted versus ℓ_o/h_c ratio in a bar chart given in Fig. 21. It is clear from Fig. 21 that for specimens with $\ell_o/h_c < 1.5$, reduction in peak load was in the range of 6%; however, loss of stiffness was in the range of 15%. It is therefore recommended in this study to classify openings with $\ell_o/h_c < 1.5$ as "small" openings in which percentage loss of peak load and stiffness would be minor and within acceptable range compared to solid beams (with no openings). In this case, strengthening may not be needed to restore the original beam capacity. For unstrengthened beams with $1.5 \leq \ell_o/h_c \leq 4.0$, reduction in peak load and stiffness ranged from 23% to 65% and 34% to 69%, respectively, as seen in Fig. 21. Openings with $1.5 \leq \ell_o/h_c \leq 4.0$ may be

Table 5
Details and FE results of beams used in the parametric study.*

Beam ID	Opening Size (mm)		ℓ_o/h_c	Strengthening scheme	FE results								
	h_o	ℓ_o			P_y (kN)	P_u (kN)	Δ_y (mm)	Δ_u (mm)	K_s (kN/mm)	$\mu\Delta$	E_u (kN.m)	ε_{su} ($\mu\varepsilon$)	Failure mode
Effect of steel plate parameters													
BS2-O1	225	450	4	Scheme-2	222	231	17.7	39.3	12.5	2.2	7.1	13,956	Y-BKL-SF
BS3-O1	225	450	4	Scheme-3	220	235	16.6	43.8	13.2	2.6	8.3	30,770	Y-SF
BS4-O1	225	450	4	Scheme-4	221	236	16.0	48.6	13.8	3.0	9.5	36,352	Y-SF
BS2-O2	225	675	6	Scheme-2	NY	151	NY	43.6	5.7	–	4.9	2120	BKL-SF
BS3-O2	225	675	6	Scheme-3	NY	155	NY	37.5	6.7	–	4.6	2142	SF
BS4-O2	225	675	6	Scheme-4	NY	166	NY	36.5	7.4	–	4.5	2165	SF
Effect of opening size													
BU-0.0†	No opening		0	Unstrengthened	226	238	9.4	85.7	24.2	9.1	18.2	69,540	Y-CC
BU-0.67	225	75	0.67	Unstrengthened	219	238	9.8	64.1	22.3	6.5	14.0	60,309	Y-CC
BU-1.0	225	113	1.00	Unstrengthened	219	238	9.7	56.7	22.5	5.8	12.2	58,181	Y-CC
BU-1.11	225	125	1.11	Unstrengthened	218	237	10.1	48.9	21.5	4.8	10.3	46,435	Y-SF
BU-1.33	225	150	1.33	Unstrengthened	217	224	13.0	16.6	20.6	1.3	2.6	4888	Y-SF
BU-1.5	225	169	1.50	Unstrengthened	NY	183	NY	12.2	15.9	–	1.5	2362	SF
BU-1.78	225	200	1.78	Unstrengthened	NY	139	NY	12.4	13.9	–	1.3	1783	SF
BU-2.0	225	225	2.00	Unstrengthened	NY	138	NY	11.3	13.4	–	1.1	1781	SF
BS-2.0	225	225	2.00	Scheme-4	220	239	10.7	68.2	20.6	6.4	14.8	60,724	Y-CC
BU-2.44	225	275	2.44	Unstrengthened	NY	132	NY	11.5	12.6	–	1.1	1714	SF
BS-2.44	225	275	2.44	Scheme-4	220	238	11.3	66.8	19.4	5.9	14.5	57,242	Y-CC
BU-3.0	225	338	3.00	Unstrengthened	NY	118	NY	11.3	11.0	–	0.9	1530	SF
BS-3.0	225	338	3.00	Scheme-4	220	238	12.1	66.1	18.2	5.5	14.2	54,118	Y-CC
BU-3.5	225	394	3.50	Unstrengthened	NY	111	NY	12.3	9.5	–	0.9	1431	SF
BS-3.5	225	394	3.50	Scheme-4	216	237	14.6	48.1	14.8	3.3	9.7	40,524	Y-SF
BU-4.0**	225	450	4.00	Unstrengthened	NY	83	NY	11.4	7.5	–	0.7	961	SF
BS-4.0***	225	450	4.00	Scheme-4	221	236	16.0	48.6	13.8	3.0	9.5	36,352	Y-SF
BU-4.5	225	506	4.50	Unstrengthened	NY	70	NY	11.8	6.6	–	0.6	837	SF
BS-4.5	225	506	4.50	Scheme-4	NY	197	NY	29.4	9.9	–	4.9	2551	SF
BU-5.0	225	563	5.00	Unstrengthened	NY	70	NY	13.7	5.2		0.6	810	SF
BS-5.0	225	563	5.00	Scheme-4	NY	183	NY	33.5	8.2	–	4.7	2424	SF
BU-6.0+	225	675	6.00	Unstrengthened	NY	70	NY	18.4	3.9	–	0.8	718	SF
BS-6.0++	225	675	6.00	Scheme-4	NY	166	NY	36.5	7.4	–	4.5	2165	SF
BU-6.44	225	725	6.44	Unstrengthened	NY	69	NY	25.4	2.8	–	1.2	1027	SF
BS-6.44	225	725	6.44	Scheme-4	NY	117	NY	40.3	3.9	–	3.8	1826	SF

* h_o = depth of opening; ℓ_o = length of opening; h_c = larger of h_b and h_t where h_b & h_t = depth of bottom and top chords, respectively; P_y and Δ_y = load and mid-span deflection at yielding of main steel, respectively; P_u = ultimate load; Δ_u = mid-span deflection at ultimate state; K_s = effective pre-yield stiffness; μ_Δ = deflection ductility ratio = Δ_u/Δ_y; E_u = energy dissipated at ultimate state; ε_{su} = peak strain in bottom rebars at mid-span; Y-BKL-SF = steel yielding at mid-span followed by out-of-plane buckling of steel plates and finally shear failure at opening; Y-SF = steel yielding at mid-span followed shear failure at opening; BKL-SF = out-of-plane buckling of steel plates followed by shear failure at opening; SF = shear failure at opening; Y-CC = steel yielding followed by concrete crushing at mid-span; NY = No steel yielding.
† Same as control beam BC-N.
** Same as beam BC-O1.
*** Same as beam BS4-O1.
+ Same as beam BC-O2.
++ Same as beam BS4-O2.

therefore classified as "large". For openings with $\ell_o/h_c > 4.0$, loss of peak load due to opening was found to be about 71% for all specimens. Openings with $\ell_o/h_c > 4.0$ are then recommended to be classified as "very large". In cases of large and very large openings, strengthening is necessary in order to fully or partially restore the original beam strength and stiffness.

Fig. 22 depicts the effect of opening size on load-deflection curves of strengthened beams. Fig. 23 presents a bar chart with percentage losses of peak load, stiffness and energy dissipated due to opening plotted versus ℓ_o/h_c ratio for strengthened beams. Plots for unstrengthened beams are also given in Fig. 23 for comparison. As seen from Figs. 22 and 23(a) and from Table 5, for beams with large openings, strengthening scheme-4 was successful in almost restoring the original beam capacity. Flexural failure was noticed for strengthened beams with $\ell_o/h_c \leq 3.0$; however, yielding of main tension steel was predicted for strengthened specimens with $\ell_o/h_c \leq 4.0$. As seen from Fig. 23(a), for very large openings ($\ell_o/h_c > 4.0$), efficiency of strengthening scheme-4 is reduced with increase in opening size. Loss of peak load due to opening increased from 17% for $\ell_o/h_c = 4.5$ to 51% for $\ell_o/h_c = 6.44$. As seen from Figs. 22 and 23(b), original beam stiffness could not be fully restored by strengthening. For beams with large openings,

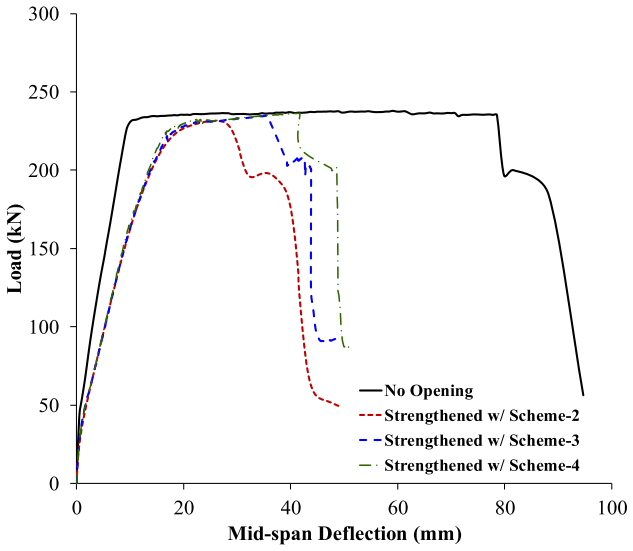

Fig. 19. Effect of steel plate parameters on load-deflection curves of strengthened beams with 450 mm opening (based on FE analysis).

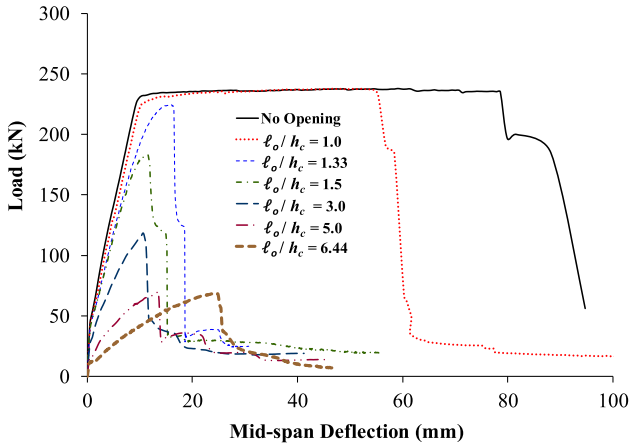

Fig. 20. Effect of opening size on load-deflection curves of unstrengthened beams (based on FE analysis).

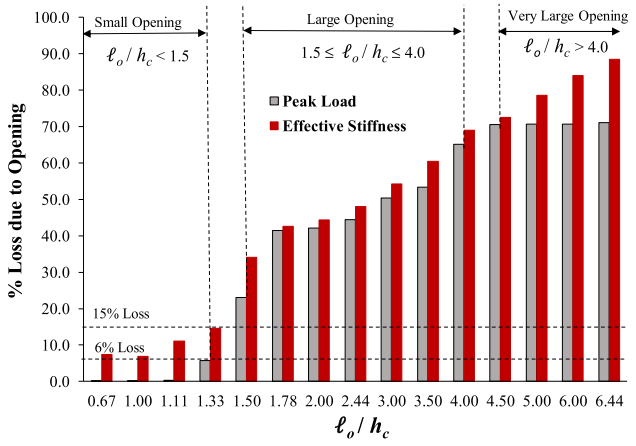

Fig. 21. Effect of opening size on peak load and effective stiffness of unstrengthened beams.

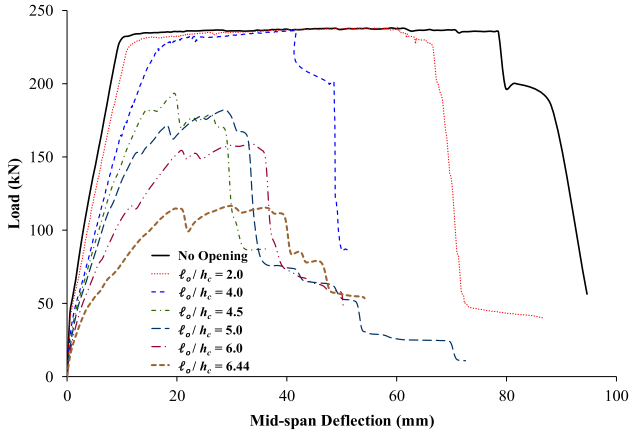

Fig. 22. Effect of opening size on load-deflection curves of strengthened beams (based on FE analysis).

strengthening scheme-4 could restore from 57% to 85% of the original beam stiffness. However, for beams with very large openings, strengthening scheme-4 could only restore from 16% to 40% of the original beam stiffness. Fig. 23(c) and Table 5 illustrate that for beams with large openings, strengthening scheme-4 could significantly enhance the energy dissipated at ultimate state compared to unstrengthened beams. However, the effect of strengthening on energy dissipated was very limited for beams with very large openings as loss of energy due to opening ranged from 73% to 79% as seen in Fig. 23(c).

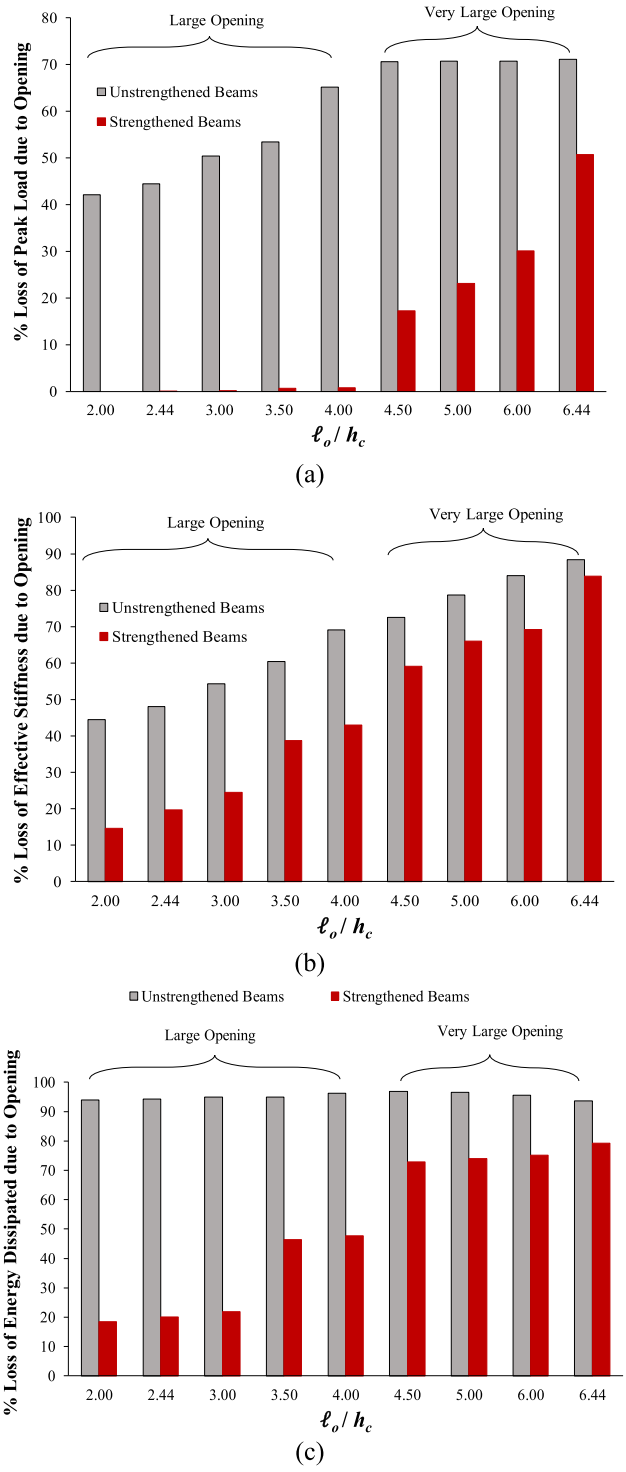

Fig. 23. Effect of opening size on performance of unstrengthened and strengthened beams with respect to: (a) peak load; (b) effective stiffness; (c) energy dissipated at ultimate state.

7. Conclusions and recommendations

The major conclusions drawn from the experimental and FE study presented in the paper are:

1) The FE modeling used in this study was found appropriate in assessing the strength and stiffness of both unstrengthened and FRP-strengthened RC beams with large rectangular web openings in shear zones. This demonstrates the usefulness of the FE modeling methods that may be used with greater confidence in future research on the employment of FRP materials for upgrading RC members.
2) Rectangular web openings in the shear zones of RC beams can be classified as small, large or very large, based on the ℓ_o/h_c ratio, where ℓ_o is the length of the opening and h_c is the larger of h_b (depth of bottom chord) and h_t (depth of top chord). Openings with $\ell_o/h_c < 1.5$ can be classified as small. However, large openings are those with $1.5 \leq \ell_o/h_c \leq 4.0$. Openings with $\ell_o/h_c > 4.0$ are recommended to be classified as very large.
3) For small rectangular web openings in the shear zones of RC beams, loss of strength and stiffness due to opening is minor and within acceptable range compared to solid beams (with no openings). In this case, strengthening may not be needed. For beams with large rectangular openings in the shear zones, FRP strengthening may be used to fully restore the strength and to partially restore the stiffness. The proposed scheme-4 of this study (with steel plate thickness of 3% of the beam width and spacing between rods less than the maximum pitch that could prevent elastic buckling of the steel plate) is recommended in this case. However, for beams with very large openings, strengthening may not be efficient to fully restore the original beam strength.

Conflict of interest

None.

Acknowledgements

The Authors would like to extend their sincere appreciation to the Deanship of Scientific Research at King Saud University for its funding of this research through the research group project No. RGP-VPP-104.

References

[1] E.G. Prentzas, Behavior and Reinforcement of Concrete Beams with Large Rectangular Apertures PhD Thesis, University of, Sheffield, UK, 1968, p. 230.
[2] M.A. Mansur, Effect of openings on the behavior and strength of R/C beams in shear, Cem. Concr. Compos. 20 (1998) 477–486.
[3] M.A. Mansur, K. Tan, W. Wei, Effects of creating an opening in existing beams, ACI Struct. J. 96 (6) (1999) 899–906.
[4] K.H. Tan, M.A. Mansur, L. Huang, Reinforced concrete T-beams with large web openings in positive and negative moment regions, ACI Struct. J. 93 (3) (1996) 277–289.
[5] K. Soudki, E. El-Salakawy, B. Craig, Behavior of CFRP strengthened reinforced concrete beams in corrosive environment, ASCE J. Compos. Constr. 11 (3) (2007) 291–298.
[6] R. El-Hacha, M. Green, G. Wight, Effect of severe environmental exposures on CFRP wrapped concrete columns, ASCE J. Compos. Constr. 14 (1) (2010) 83–93.
[7] Y.A. Al-Salloum, Influence of edge sharpness on the strength of square concrete columns confined with composite laminates, Compos. Part B-Eng. 38 (2007) 640–650.
[8] Y.A. Al-Salloum, N.A. Siddiqui, H.M. Elsanadedy, A.A. Abadel, M.A. Aqel, Textile-reinforced mortar (TRM) versus FRP as strengthening material of seismically deficient RC beam-column joints, ASCE J. Compos. Constr. 15 (6) (2011) 875–1002.
[9] Y.A. Al-Salloum, H.M. Elsanadedy, S.H. Alsayed, R. Iqbal, Experimental and numerical study for the shear strengthening of RC beams using textile reinforced mortar, ASCE J. Compos. Constr. 16 (1) (2012) 74–90.
[10] S.H. Alsayed, T.H. Almusallam, Y.A. Al-Salloum, N.A. Siddiqui, Seismic rehabilitation of corner RC beam-column joints using CFRP composites, ASCE J. Compos. Constr. 14 (6) (2010) 681–692.
[11] S.H. Alsayed, T.H. Almusallam, S.M. Ibrahim, N.M. Al-Hazmi, Y.A. Al-Salloum, H. Abbas, Experimental and numerical investigation for compression response of CFRP strengthened shape modified wall-like RC column, Constr. Build. Mater. 63 (2014) 72–80.
[12] H.M. Elsanadedy, Y.A. Al-Salloum, Z.M. Al-Zaheri, S.H. Alsayed, H. Abbas, Behavior and design aspects of FRP-strengthened URM walls under out-of-plane loading. ASCE, J. Compos. Constr. 20 (6) (2016).
[13] H.M. Elsanadedy, T.H. Almusallam, S.H. Alsayed, Y.A. Al-Salloum, Experimental and FE study on RC one-way slabs upgraded with FRP composites, KSCE J. Civ. Eng. 19 (4) (2015) 1024–1040.
[14] H.M. Elsanadedy, Y.A. Al-Salloum, S.H. Alsayed, R. Iqbal, Experimental and numerical investigation of size effects in FRP-wrapped concrete columns, Constr. Build. Mater. 29 (2012) 56–72.
[15] H.M. Elsanadedy, Y.A. Al-Salloum, H. Abbas, S.H. Alsayed, Prediction of strength parameters of FRP confined concrete, Compos. Part B-Eng. 43 (2) (2012) 228–239.
[16] H.M. Elsanadedy, H. Abbas, Y.A. Al-Salloum, Almusallam TH. Prediction of intermediate crack debonding strain of externally bonded FRP laminates in RC beams and one-way slabs, ASCE J. Compos. Constr. 18 (5) (2014).
[17] T. Norris, H. Saadatmanesh, M.R. Ehsani, Shear and flexural strengthening of RC beams with carbon fiber sheets, ASCE J. Struct. Eng. 123 (7) (1997) 903–911.
[18] H. Saadatmanesh, A.M. Malek, Design guidelines for flexural strengthening of RC beams with FRP plates, ASCE J. Compos. Constr. 2 (4) (1998) 158–164.
[19] H.A. Abdalla, A.M. Torkey, H.A. Haggag, A.F. Abu-Amira, Design against cracking at openings in reinforced concrete beams strengthened with composite sheets, Compos. Struct. 60 (2) (2003) 197–204.
[20] A. Pimanmas, Strengthening R/C beams with opening by externally installed FRP rods: Behavior and analysis, Compos. Struct. 92 (2010) 1957–1976.
[21] T. El Maaddawy, S. Sherif, FRP composites for shear strengthening of reinforced concrete deep beams with openings, Compos. Struct. 89 (2009) 60–69.
[22] R. Hawileh, T.A. El-Maaddawy, M. Naser, Non-linear finite element modeling of concrete deep beams with openings strengthened with externally-bonded composites, Mater. Des. 42 (2012) 378–387.
[23] X.F. Nie, S.S. Zhang, J.G. Teng, G.M. Chen, Experimental study on RC T-section beams with an FRP-strengthened web opening, Compos. Struct. 185 (2018) 273–285.
[24] Livermore Software Technology Corporation (LSTC), LS-DYNA User's Keyword Manual (Nonlinear Dynamic Analysis of Structures in Three Dimensions) Volume 1. Version 971, LSTC, Livermore, CA, 2007.
[25] ASTM, Standard Test Method for Compressive Strength of Cylindrical Concrete Specimens. ASTM C39/C39M – 17, American Society for Testing and Materials, West Conshohocken, PA, USA, 2017.
[26] ASTM, Standard Test Methods for Tension Testing of Metallic Materials. ASTM E8E8M – 16a, American Society for Testing and Materials, West Conshohocken, PA, USA, 2016.
[27] ASTM, Standard Test Methods and Definitions for Mechanical Testing of Steel Products. ASTM A370 – 17, American Society for Testing and Materials, West Conshohocken, PA, USA, 2017.
[28] ASTM, Standard Test Method for Tensile Properties of Polymer Matrix Composite Materials. ASTM D3039/D3039M – 14, American Society for Testing and Materials, West Conshohocken, PA, USA, 2014.
[29] NZS 4203: 1992. New Zealand Standard, Code of practice for general structural design and design loadings for buildings 1, 1992.
[30] T.B. Belytschko, C.S. Tsay, Explicit algorithms for non-linear dynamics of shells, J. Appl. Mech. Appl. Mech. Div. ASME 48 (1981) 209–231.
[31] Y.D. Murray, User's Manual for LS-DYNA Concrete Material Model 159. Report No. FHWA-HRT-05-062, US Department of Transportation, Federal Highway Administration National Transportation Systems Center, USA, 2007.
[32] Y.D. Murray, A. Abu-Odeh, R. Bligh, Evaluation of Concrete Material Model 159. Report No. FHWA-HRT-05-063, US Department of Transportation, Federal Highway Administration National Transportation Systems Center, USA, 2007.
[33] F.K. Chang, K.Y. Chang, A progressive damage model for laminated composites containing stress concentration, J. Compos. Mater. 21 (1987) 834–855.
[34] J.F. Chen, J.G. Teng, Anchorage strength models for FRP and steel plates bonded to concrete, ASCE J. Struct. Eng. 127 (7) (2001) 784–791.
[35] X.Z. Lu, J.G. Teng, L.P. Ye, J.J. Jiang, Bond-slip models for sheets/plates bonded to concrete, Eng. Struct. 27 (6) (2005) 920–937.
[36] H.M. Elsanadedy, T.H. Almusallam, S.H. Alsayed, Y.A. Al-Salloum, Flexural strengthening of RC beams using textile reinforced mortar – experimental and numerical study, Compos. Struct. 97 (2013) 40–55.
[37] T.H. Almusallam, H.M. Elsanadedy, Y.A. Al-Salloum, Effect of longitudinal steel ratio on behavior of RC beams strengthened with FRP composites – experimental and FE study, ASCE J. Compos. Constr. 19 (1) (2015).
[38] M. Mansur, K.H. Tan, in: Concrete beams with openings: Analysis and design, CRC Press, 1999, p. 224.